Acta Pharmaceutica Sinica B 2026;16(8):5405−5423

Chinese Pharmaceutical Association
Institute of Materia Medica, Chinese Academy of Medical Sciences

Acta Pharmaceutica Sinica B

www.elsevier.com/locate/apsb
www.sciencedirect.com

ORIGINAL ARTICLE

Universal off-the-shelf TGF-β1-knockout whole-tumor cell vaccine overcomes immunotherapy resistance in pMMR/MSS tumors

Weixiao Yang[a,†], Zhexu Dong[a,†], Qi Xiong[a], Yushuang Ren[a], Lin Zhang[a], Yi Liu[b], Jiaqi Han[a], Tian Tian[c], Xiaolan Su[a], Gang Shi[a,*], Hongxin Deng[a,*]

[a]*Department of Biotherapy, Cancer Center and State Key Laboratory of Biotherapy, West China Hospital, Sichuan University, Chengdu 610041, China*
[b]*Geriatrics Research Institute, Sichuan Provincial People's Hospital, School of Medicine, University of Electronic Science and Technology of China, Chengdu 610072, China*
[c]*Department of Radiation Oncology, Yunnan Cancer Hospital & the Third Affiliated Hospital of Kunming Medical University & Peking University Cancer Hospital, Kunming 650118, China*

Received 4 November 2025; received in revised form 14 January 2026; accepted 2 February 2026

KEY WORDS

Whole-tumor-cell vaccine;
TGF-β1 knockout;
Poly(I:C);
pMMR/MSS tumors;
Immunotherapy;
Immune checkpoint blockade;
Adaptive immune priming;
Antigen presentation

Abstract Mismatch repair-proficient (pMMR)/microsatellite-stable (MSS) tumors, representing the majority of solid cancers, remain largely unresponsive to immune checkpoint inhibitors, highlighting the urgent need for effective therapeutic strategies. Tumor cell vaccines, serving as delivery platforms for a broad repertoire of tumor antigens, hold potential for eliciting systemic antitumor immunity, yet their clinical efficacy has remained limited. Here, we developed Tβ1KO/PolyIC-Vac, an off-the-shelf therapeutic whole-tumor cell vaccine generated by CRISPR-Cas9-mediated TGF-β1 knockout and formulated with the TLR3 agonist Poly(I:C). In therapeutic vaccination models, subcutaneous vaccination significantly suppressed distal tumor growth, reduced lung metastases, and delayed spontaneous colorectal tumor progression. It also synergized with anti-PD-1 blockade, enhancing complete response rates and establishing baseline antitumor immunity. Mechanistically, knockout of tumor-derived TGF-β1 reprogrammed immunity by reducing MDSC accumulation to relieve local immunosuppression and activate dendritic cells in draining lymph nodes, while intrinsically triggering the tumor STAT1−IL-15 axis

*Corresponding authors.
E-mail addresses: shig2019@wchscu.edu.cn (Gang Shi), denghongx@scu.edu.cn (Hongxin Deng).
†These authors made equal contributions to this work.
Peer review under the responsibility of Chinese Pharmaceutical Association and Institute of Materia Medica, Chinese Academy of Medical Sciences.

https://doi.org/10.1016/j.apsb.2026.06.001

to enhance vaccine immunogenicity. Poly(I:C) further enhanced cross-presentation and adaptive immunity, conferring long-term cross-protection against heterologous tumors. Together, these findings establish Tβ1KO/PolyIC-Vac as a universal tumor vaccine platform capable of efficiently delivering a comprehensive repertoire of tumor antigens and eliciting robust, durable, and cross-protective tumor-specific immunity in immunotherapy-resistant pMMR/MSS tumors.

1. Introduction

Cancer immunotherapy, including immune checkpoint blockade (ICB), chimeric antigen receptor (CAR) T cells, and therapeutic cancer vaccines, has transformed cancer treatment by restoring antitumor immune responses[1−5]. However, most solid tumors (>90%) exhibit proficient mismatch repair (pMMR) or microsatellite stability (MSS) and respond poorly to current immunotherapies[6,7]. In colorectal cancer (CRC), only ∼15% of patients with dMMR/MSI-H tumors benefit from PD-1 blockade, whereas ∼85% with pMMR/MSS tumors show limited efficacy[8−10]. Similar resistance is observed in pMMR−type gastric[11], endometrial[12,13], and prostate cancers[14]. This resistance stems primarily from impaired dendritic cell (DC) activation, insufficient T cell priming, and a paucity of baseline tumor-reactive T cells[15−17], underscoring the need for approaches that can initiate de novo antitumor immunity in pMMR/MSS tumors.

Therapeutic cancer vaccines have emerged as a promising approach to enhance tumor antigen presentation and induce tumor-specific immune responses[18,19]. Recent advances in neoantigen-based peptide and mRNA vaccines have demonstrated clinical potential, yet these personalized strategies are limited by technical complexity, high cost, and restricted accessibility, highlighting the need for universal, off-the-shelf platforms[20,21]. Whole-cell tumor vaccines represent a promising platform by presenting a broad repertoire of tumor antigens, including shared targets[22−26]. Despite robust prophylactic efficacy in preclinical models, their therapeutic benefit remains limited[27]. This limitation is especially notable in mismatch repair-proficient (pMMR) tumors, which exhibit strong immune evasion and present a central barrier to the engineering of whole-tumor cell vaccines. Attempts to improve efficacy through cytokine overexpression (*e.g.*, GM-CSF) have yielded limited clinical success, likely because irradiation-mediated tumor cell inactivation attenuates cytokine expression, thereby limiting therapeutic efficacy[28]. In comparison, immune-stimulatory adjuvant formulation offers a reliable and robust approach to augment vaccine efficacy[29]. In addition, CD47 knockout has been reported to enhance vaccine efficacy when administered intrasplenically, whereas its benefit was markedly reduced with subcutaneous administration[30]. These findings underscore the necessity of next-generation vaccine designs that integrate suppression relief with immune stimulation, which is essential for improving the immunogenicity of pMMR tumor cell-based vaccines.

Transforming growth factor β1 (TGF-β1) is widely upregulated across tumor types and promotes immune evasion by suppressing antigen presentation, inhibiting T cell activation, and diminishing tumor-intrinsic immunogenicity through processes such as epithelial-mesenchymal transition and PD-L1 induction[31−34]. Targeting TGF-β signaling has been shown to enhance the sensitivity of pMMR/MSS colorectal cancers to PD-1/PD-L1 blockade, highlighting TGF-β1 as an attractive target for overcoming immunosuppression[35]. Nevertheless, whether complete TGF-β1 ablation can enhance the antigen-presenting efficiency and immune priming capacity of pMMR tumor cell vaccines remains unclear.

To address these challenges, we developed Tβ1KO/PolyIC-Vac, a therapeutic whole-tumor-cell vaccine generated from pMMR tumor cells with CRISPR-mediated knockout of TGF-β1, serving as an antigen-delivery platform and formulated with the TLR3 agonist Poly(I:C) as an adjuvant. Subcutaneous vaccination (i) suppressed distal pMMR tumor growth and reduced pulmonary metastases, (ii) induced cross-protective immunity against spontaneous and heterologous tumors, and (iii) enhanced the efficacy of PD-1 blockade by establishing baseline antitumor immunity. Mechanistically, knockout of tumor-derived TGF-β1 exerted a dual immunomodulatory effect—simultaneously reducing MDSC accumulation at the vaccination site to relieve local immunosuppression, and intrinsically activating the tumor STAT1/IL-15 axis to drive potent dendritic cell activation. The Poly(I:C) adjuvant further polarized cDC1 cells toward an interferon-producing state in draining lymph nodes, thereby amplifying $CD8^+$ T cell and plasma cell mediated antitumor immunity. Collectively, these findings establish Tβ1KO/PolyIC-Vac as a promising universal "off-the-shelf" vaccine platform for immunotherapy-resistant pMMR/MSS tumors.

2. Materials and methods

2.1. Reagents

Polyinosinic−polycytidylic acid [Poly(I:C), high molecular weight] (InvivoGen, San Diego, CA, USA), azoxymethane (AOM) (MilliporeSigma, Burlington, MA, USA), and dextran sodium sulfate (DSS) (MP Biomedicals, Irvine, CA, USA) were used as indicated. Lipofectamine 3000 transfection reagent (Thermo Fisher Scientific, Waltham, MA, USA) and puromycin (Beyotime, Shanghai, China) were used for gene transduction and selection. Collagenase type IV (Gibco, Grand Island, NY, USA), dispase (Solarbio, Beijing, China), Benzonase nuclease (Sino Biological, Beijing, China), and ACK red blood cell lysis buffer (Solarbio, Beijing, China) were used for tissue dissociation and cell preparation. Fixable Viability Stain 700 (BD Biosciences, San Jose, CA, USA) and Fc receptor blocker (Selleck Chemicals, Houston, TX, USA) were used for flow cytometry staining. The BD Cytofix/Cytoperm fixation/permeabilization kit (BD Biosciences, San Jose, CA, USA) was used for intracellular staining. The CRISPR/Cas9 lentiviral backbone pLentiCRISPR v2 (Addgene, Watertown, MA, USA) and sgRNA oligonucleotides targeting murine

Tgfb1 synthesized by TSINGKE Biotechnology (Beijing, China), were used for gene editing. An anti−PD-1 antibody (InvivoGen, San Diego, CA, USA) was administered in combination with Tβ1KO/PolyIC-Vac for combination therapy. The PE-conjugated MHC class I tetramer H-2K^d/SPSYVYHQF (MBL International, Woburn, MA, USA) was used to detect antigen-specific CD8$^+$ T cells. All chemicals and reagents were of analytical grade and used according to the manufacturers' instructions.

2.2. Studies in humans and animals

Female C57BL/6JGpt and BALB/cJGpt mice were purchased from Beijing HFK Bioscience Co., Ltd. (Beijing, China) and maintained under specific pathogen-free (SPF) conditions. Female BALB/cA-nu mice were purchased from GemPharmatech Co., Ltd. (Nanjing, China) and also housed under SPF conditions. Mice aged 6−7 weeks were used in all experiments. In each study, mice were age-matched and randomly assigned to different experimental groups.

All animal experiments were performed in strict accordance with the Guidelines for the Care and Use of Laboratory Animals and were approved by the Animal Ethics Committee of West China Hospital, Sichuan University (Approval No. 20240322005). Humane endpoints were established to minimize animal suffering, and all mice were humanely euthanized at the defined endpoints.

Human colorectal cancer tissue microarrays (HColA160Su02; Shanghai Outdo Biotechnology, Shanghai, China) were purchased for immunohistochemical analysis. No human participants, freshly collected tissues, or identifiable personal data were involved in this study. Therefore, informed consent was not required. All procedures complied with institutional ethical regulations and were conducted in accordance with the principles of the Declaration of Helsinki and the ARRIVE guidelines.

2.3. Cell lines

Human colorectal cancer (CRC) cell lines SW480 and HCT116, the mouse CRC cell line CT26, and the mouse melanoma cell line B16F10 were obtained from the American Type Culture Collection (ATCC, Manassas, VA, USA). The mouse CRC cell line MC38 was purchased from the Cell Bank of the Chinese Academy of Sciences (Shanghai, China). All cell lines were cultured in Dulbecco's modified Eagle's medium (DMEM) supplemented with 10% fetal bovine serum (FBS) (Gibco, Grand Island, NY, USA) at 37 °C in a humidified incubator with 5% CO_2. Cells were routinely tested for mycoplasma contamination using a mycoplasma detection kit (HANBIO, Shanghai, China), and no contamination was detected throughout the study.

2.4. CRISPR/Cas9-targeted Tgfβ1 gene knockout in tumor cells

Single-guide RNAs (sgRNAs) targeting exon 1 of the murine *Tgfb1* gene (sgRNA1: TGTACAACAGCACCCGCGACCGG; sgRNA2: TTAGCATAGTAGTCCGCTTC GGG) were designed using an online CRISPR design tool (http://crispr.dbcls.jp/) and cloned into the BsmBI site of the pLentiCRISPR v2 vector (Addgene, Watertown, MA, USA). Lentiviral particles were produced and transduced into CT26, MC38, and B16F10 cells using Lipofectamine 3000 transfection reagent (Thermo Fisher Scientific, Waltham, MA, USA). Forty-eight hours after transduction, cells were selected with puromycin (Beyotime, Shanghai, China) to generate stable *Tgfb1*-knockout cell lines.

2.5. Subcutaneous tumor model

Wild-type CT26, B16F10, or MC38 cells (5×10^5 cells in 100 μL sterile PBS) were subcutaneously injected into the right flank of mice. Tumor growth was measured twice weekly using digital calipers, and tumor volume was calculated as Eq. (1):

$$\text{Tumor volume}\left(\text{mm}^3\right) = (\text{Short diameter})^2 \times (\text{Long diameter}) \,/\, 2 \quad (1)$$

Mice were euthanized when tumor volume exceeded 2000 mm^3 or when clinical distress was observed, following institutional animal welfare guidelines.

2.6. Lung metastasis model

Female BALB/c mice (6 weeks old) were injected intravenously with wild-type CT26 cells (1×10^5 cells per mouse) *via* the tail vein to establish pulmonary metastases. On Day 20, mice were euthanized, and lungs were fixed in Bouin's solution for 72 h. Metastatic nodules on the lung surfaces were counted under blinded conditions to quantify metastasis.

2.7. Therapeutic tumor-cell vaccination

Tumor-bearing mice were immunized subcutaneously on Days 4, 7, and 10 after tumor inoculation at a site contralateral to the tumor. All tumor cells (wild-type or *Tgfb1*-knockout) were inactivated by irradiation at a dose of 60 Gy and resuspended in 100 μL phosphate-buffered saline (PBS). Vaccines were formulated as follows: 1×10^6 irradiated tumor cells alone (WT Vac or Tβ1KO Vac), 1×10^6 irradiated tumor cells combined with 25 μg polyinosinic−polycytidylic acid [Poly(I:C)] (WT/PolyIC Vac or Tβ1KO/PolyIC Vac), or 25 μg Poly(I:C) alone (InvivoGen, San Diego, CA, USA). For combination therapy, an anti-PD-1 antibody (200 μg; InvivoGen, San Diego, CA, USA) was administered intraperitoneally on Days 5, 8, and 11. Tumor volumes were measured every 3 Days. Mice were euthanized when tumor volumes exceeded 2000 mm^3 for survival analysis.

2.8. AOM/DSS-induced colitis-associated cancer model

The azoxymethane/dextran sodium sulfate (AOM/DSS)-induced colitis-associated cancer model was established as previously described[36]. Mice received an intraperitoneal injection of azoxymethane (10 mg/kg body weight; MilliporeSigma, Burlington, MA, USA) at 6 weeks of age. One week later, 2% dextran sodium sulfate (DSS; MP Biomedicals, Irvine, CA, USA) was administered in the drinking water until an approximately 2% loss of body weight was observed. By Day 28, precancerous lesions were confirmed by colonoscopy. Mice were then randomized into four treatment groups: phosphate-buffered saline (PBS), polyinosinic−polycytidylic acid [Poly(I:C)] alone, Tβ1KO Vac, or Tβ1KO/PolyIC Vac. Subcutaneous vaccination was initiated on Day 28, with three doses administered at 3-day intervals per treatment cycle. A second treatment cycle was performed on Day 60. On Day 75, mice were euthanized, and colorectal tissues were collected for quantification of tumor number and volume.

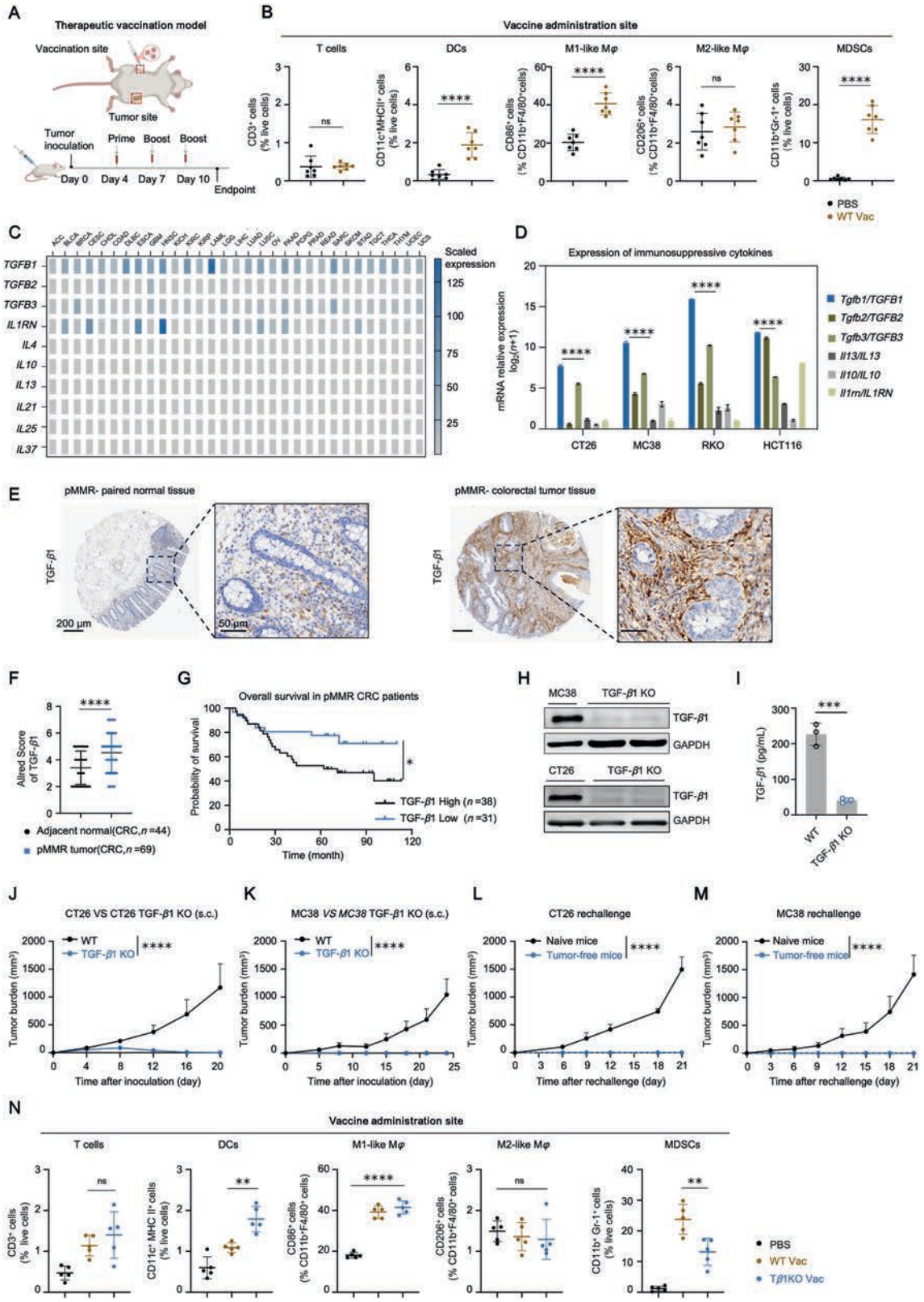

Figure 1 Knockout of TGF-β1 reverses the immunosuppressive microenvironment at the vaccination site of whole-pMMR tumor-cell vaccines. (A) Schematic of the therapeutic tumor vaccination model. Tumor-bearing mice were subcutaneously immunized with irradiated whole-cell tumor vaccines on Days 4, 7, and 10 after tumor inoculation. Tumor growth was monitored until endpoint. (B) Flow cytometric analysis of immune cell composition at the vaccination site 3 Days after treatment with PBS or CT26 WT Vac ($n = 7$). Shown are the percentages of T cells ($CD3^+$), dendritic cells ($CD11c^+MHCII^+$), M1-like macrophages ($CD11b^+F4/80^+CD86^+$), M2-like macrophages ($CD11b^+F4/80^+CD206^+$), and myeloid-derived suppressor cells ($CD11b^+Gr\text{-}1^+$). (C) Heatmap showing *TGFB1* and other immunosuppressive cytokine expression across TCGA

2.9. Tumor rechallenge and immune-memory evaluation

Mice that achieved complete tumor regression following Tβ1KO/PolyIC-Vac therapy and remained tumor-free for 3 months were rechallenged subcutaneously with CT26 or 4T1 cells (5×10^5 cells per mouse). Age-matched näive BALB/c mice served as controls. Tumor growth was monitored every 3 Days post-rechallenge. On Day 18, mice were euthanized, and spleens were collected for flow cytometric analysis of memory T-cell populations.

2.10. Detection of MuLV gp70 antigen-specific CD8$^+$ T cells by MHC tetramer staining

Single-cell suspensions were prepared from spleens after red blood cell lysis using ACK lysis buffer. To detect CT26 tumor antigen (MuLV gp70)-specific CD8$^+$ T cells, splenocytes were stained with a PE-conjugated H-2K^b/SPSYVYHQF tetramer (MBL International, Woburn, MA, USA) for 20 min at room temperature in the dark, followed by staining with a FITC-conjugated anti-mouse CD8α antibody (BioLegend, San Diego, CA, USA). Cells were analyzed by flow cytometry, and the frequency of MuLV gp70-specific CD8$^+$ T cells was quantified as the percentage of tetramer-positive cells among CD8α^+ T cells.

2.11. Flow cytometry analysis

Tumor tissues were minced and digested for 1 h at 37 °C in RPMI-1640 medium (Gibco, Grand Island, NY, USA) containing 1% fetal bovine serum (FBS; ZETA Life, Menlo Park, CA, USA), 0.1% collagenase type IV (Gibco, Grand Island, NY, USA), and benzonase nuclease (Sino Biological, Beijing, China). The resulting cell suspension was filtered through a 70-μm cell strainer (Corning Falcon, Corning, NY, USA), centrifuged at 1500 rpm for 5 min using a benchtop centrifuge (Eppendorf 5424R, Eppendorf, Hamburg, Germany), and resuspended in PBS containing 1% FBS.

For spleen and lymph node samples, tissues were mechanically dissociated through a 70 μm cell strainer and treated with ACK lysis buffer (Solarbio, Beijing, China) for 15 min on ice. Cells were then stained with Fixable Viability Stain 700 (BD Biosciences, San Jose, CA, USA) for 20 min, blocked with an Fc receptor inhibitor (Selleck Chemicals, Houston, TX, USA), and labeled with the indicated antibody panels.

For vaccination administration sites, subcutaneous tissues surrounding the inoculation area were excised, finely minced, and digested in RPMI-1640 supplemented with 1% FBS, collagenase I (2 mg/mL), collagenase IV (2 mg/mL), dispase (2 mg/mL), and benzonase nuclease at 37 °C for 1 h. The digested suspension was passed through a 70 μm cell strainer, washed, and resuspended in PBS containing 1% FBS for downstream flow cytometry analysis.

For intracellular cytokine or transcription factor staining, cells were fixed and permeabilized using the Cytofix/Cytoperm fixation/permeabilization kit (BD Biosciences, San Jose, CA, USA) or the Foxp3/Transcription Factor Staining Buffer Set (Invitrogen, Carlsbad, CA, USA). The detailed antibody list is provided in Supporting Information Table S1.

2.12. RNA-seq and analysis

Total RNA from cultured tumor cells and tumor tissues collected after treatment was extracted using TRIzol reagent (Thermo Fisher Scientific, Waltham, MA, USA). RNA integrity was assessed using an Agilent 2100 Bioanalyzer (Agilent Technologies, Santa Clara, CA, USA), and only samples with RNA integrity number (RIN) values greater than 8.0 were used for subsequent analyses. RNA libraries were prepared using the Hieff NGS Ultima Dual-mode mRNA Library Prep Kit (Yeasen Biotechnology, Shanghai, China) and sequenced on an Illumina NovaSeq X Plus platform by Gene Denovo Biotechnology Co., Ltd. (Guangzhou, China), generating more than 40 million paired-end reads per sample. Differential gene expression analysis was performed using DESeq2 with thresholds of $|\log_2 \text{fold change}| > 1$ and false discovery rate (FDR) < 0.05. Gene Ontology and Kyoto Encyclopedia of Genes and Genomes (KEGG) pathway enrichment analyses were conducted using the Omicsmart platform. Heatmaps and bar plots of differentially expressed genes were generated using GraphPad Prism (version 9.2.0).

2.13. Single-cell RNA-seq library and sequencing

Draining lymph nodes on the vaccine-injected side were dissected, mechanically dissociated, and filtered through a 70 μm cell strainer to obtain single-cell suspensions. Single-cell RNA sequencing (scRNA-seq) libraries were prepared using the MobiCube Single-Cell Chip Kit V2.1 for droplet encapsulation and the MobiCube Single-Cell 3′ RNA-seq Kit for cDNA synthesis and barcoding (Mobio Technology, Shanghai, China). SPRIselect reagent (Beckman Coulter, Brea, CA, USA) was used for cDNA size selection and purification. All procedures were performed according to the manufacturers' protocols. Cells were loaded at an optimal concentration (700−1200 cells/μL) and

tumor types. Colors indicate median RNA-seq expression (TPM). (D) Quantitative PCR (qPCR) analysis of immunosuppressive cytokine expression in human (HCT116, RKO) and mouse (CT26, MC38) tumor cell lines ($n = 3$). Data are shown as $\log_2(n+1)$. (E) Representative immunohistochemistry (IHC) staining of TGF-β1 in tissue microarrays from mismatch repair-proficient (pMMR) colorectal cancer (CRC) patients. Scale bars, 200 μm (left) and 50 μm (magnified panels). (F) Quantification of TGF-β1 expression by the Allred scoring system (range 0−7) in adjacent normal ($n = 44$) and pMMR CRC tumor tissues ($n = 69$). Each dot represents one patient sample. (G) Kaplan−Meier analysis of overall survival in pMMR CRC patients stratified by TGF-β1 expression (low, $n = 31$; high, $n = 38$). (H) Western blot analysis of TGF-β1 protein expression in WT and TGF-β1-knockout (KO) MC38 and CT26 tumor cells, with GAPDH as a loading control. (I) ELISA quantification of secreted TGF-β1 protein in WT and TGF-β1 KO tumor cells. (J, K) Tumor growth curves of CT26 WT *vs*. CT26 TGF-β1 KO cells (J, BALB/c mice, $n = 6$) and MC38 WT *vs.* MC38 TGF-β1 KO cells (K, C57BL/6J mice, $n = 6$) after subcutaneous inoculation. (L, M) Tumor rechallenge experiments in CT26 (L) and MC38 (M) models. Tumor-free mice from TGF-β1 KO groups were rechallenged with the corresponding WT tumor cells. Naive mice served as controls ($n = 6$). (N) Flow cytometric analysis of immune cell subsets at the vaccination site 3 Days after immunization with PBS, CT26 WT Vac, or CT26 Tβ1KO Vac ($n = 5$). Statistical significance was determined using unpaired two-tailed Student's *t*-test for pairwise comparisons, log-rank (Mantel-Cox) test for Kaplan−Meier survival analysis, and two-way ANOVA with Bonferroni *post hoc* test for tumor growth curves. Data are shown as mean ± SD. *$P < 0.05$, **$P < 0.01$, ***$P < 0.001$, ****$P < 0.0001$ *vs*. indicated; ns, not significant.

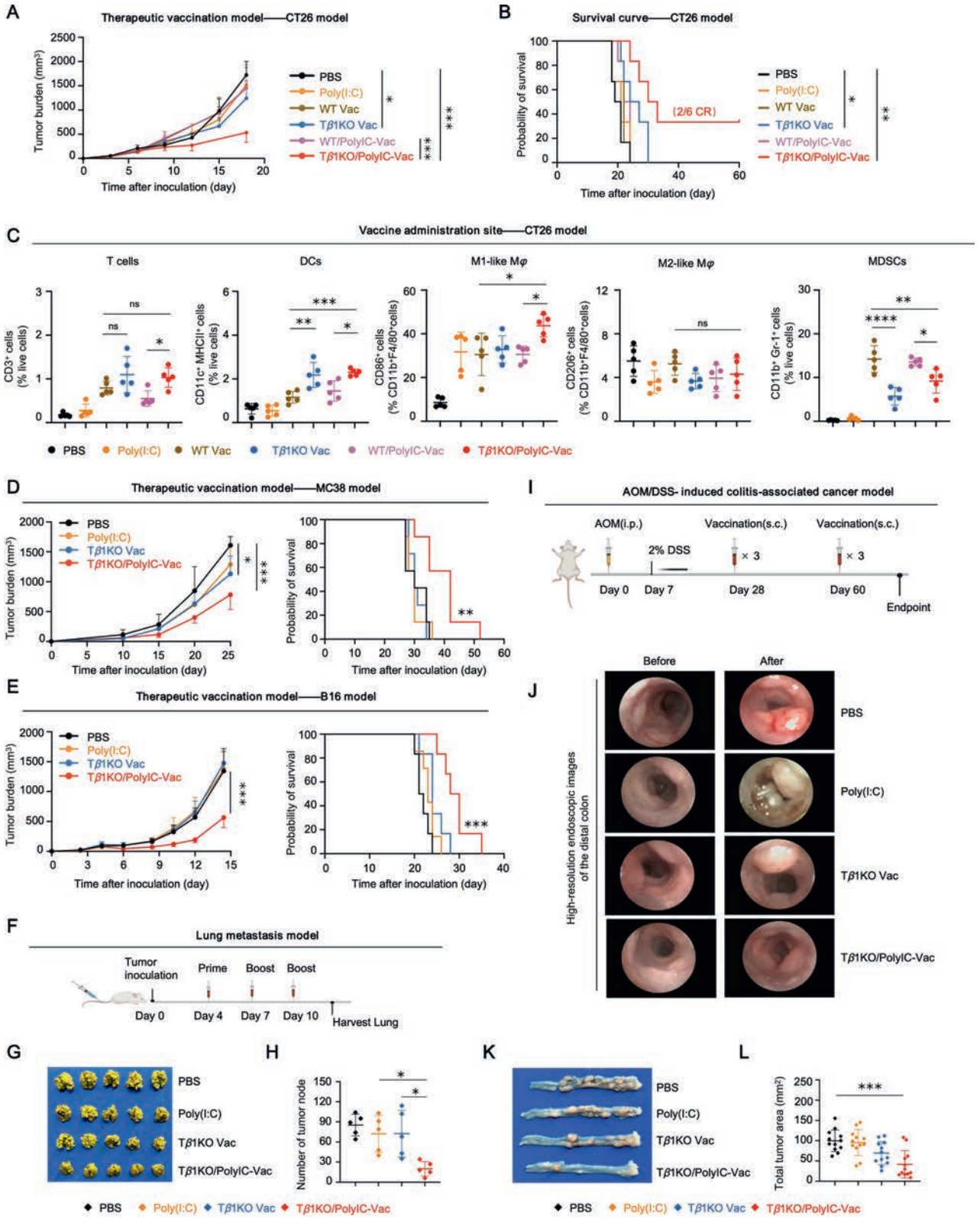

Figure 2 Therapeutic administration of Tβ1KO/PolyIC-Vac inhibits pMMR tumor growth across multiple models. (A) Tumor growth curves of CT26 tumors in mice vaccinated with PBS (black), Poly(I:C) (orange), WT Vac (brown), Tβ1KO Vac (blue), WT/PolyIC-Vac (purple), or Tβ1KO/PolyIC-Vac (red) ($n = 6$). (B) Kaplan−Meier survival curves of the treatment groups shown in (A). (C) Flow cytometric analysis of T cells ($CD3^+$), dendritic cells ($CD11c^+MHCII^+$), M1-like macrophages ($CD11b^+F4/80^+CD86^+$), M2-like macrophages ($CD11b^+F4/80^+CD206^+$), and myeloid-derived suppressor cells ($CD11b^+Gr\text{-}1^+$) at the vaccination site ($n = 5$). (D) Tumor growth curves (left) and suvival analysis (right) of MC38 therapeutic vaccination model ($n = 7$). (E) Tumor growth curves (left) and survival analysis (right) of mice bearing B16 tumors after

subjected to reverse transcription, cDNA amplification, and library construction. Gene quantification quality control was performed using MobiVision software (version 3.2) prior to sequencing. Libraries were sequenced on an Illumina platform using paired-end 150-bp reads, with a sequencing depth exceeding 50,000 reads per cell.

2.14. Statistical analysis

All data are presented as mean ± standard deviation (SD). Statistical analyses were performed using GraphPad Prism software (version 9.0), as specified in the figure legends. Differences between two groups were assessed using unpaired two-tailed Student's *t*-tests. For comparisons among multiple groups, one-way or two-way analysis of variance (ANOVA) followed by Tukey's or Bonferroni's *post hoc* test was applied, as appropriate. Survival data were analyzed using the Kaplan−Meier method and compared using the log-rank (Mantel−Cox) test. Unless otherwise stated, statistical significance is indicated as $*P < 0.05$, $**P < 0.01$, $***P < 0.001$, $****P < 0.0001$; ns, not significant.

3. Results

3.1. Irradiated wild-type pMMR tumor cell vaccines recruit immunosuppressive cells and lack therapeutic efficacy

Irradiated wild-type pMMR tumor cell vaccines show limited efficacy, in part because immunosuppressive signals may persist despite inactivation. To address this limitation, we generated an irradiated whole-cell vaccine from murine pMMR-type colorectal cancer CT26 cells (referred to as CT26 WT Vac) and assessed its antitumor efficacy following the strategy outlined in Fig. 1A. However, CT26 WT Vac did not significantly enhance immune cell infiltration within the tumor microenvironment and failed to suppress the growth of distant tumors (Supporting Information Fig. S1A−S1C, gating strategy shown in Fig. S1D). While vaccination led to increased recruitment of dendritic cells and M1-like macrophages at the vaccine administration site, there was no notable change in T cell populations. In contrast, the proportion of myeloid-derived suppressor cells (MDSCs) increased markedly (Fig. 1B, gating strategy shown in Fig. S1E). These results suggest that irradiated wild-type pMMR tumor cell vaccines may retain suppressive signals that hinder early immune activation post-vaccination, thereby limiting antitumor responses.

3.2. Targeting tumor cell-derived TGF-β1 reverses local immunosuppression at the vaccination site

Cytokine signaling networks orchestrate the recruitment and activation of immune cells. To identify dominant immunosuppressive mediators in tumor cell vaccines, we analyzed the expression of key suppressive cytokines—including *TGFB1, TGFB2, TGFB3, IL1RN, IL4, IL10, IL13, IL21, IL25,* and *IL37*—across 31 cancer types in The Cancer Genome Atlas (TCGA). Among these, *TGFB1* showed the highest expression levels in several common malignancies, including colorectal cancer (COAD), breast cancer (BRCA), lung adenocarcinoma (LUAD), gastric cancer (STAD), and ovarian cancer (OV) (Fig. 1C). This trend was also observed in pMMR tumor samples from COAD and STAD (Supporting Information Fig. S2A). Consistent with the TCGA analysis, quantitative PCR demonstrated that *TGFB1* expression was markedly elevated relative to other immunosuppressive genes in human pMMR tumor cell lines (HCT116, SW480), and *Tgfb1* expression was similarly elevated in murine cell lines (CT26, MC38) (Fig. 1D). All gene-specific primers used for quantitative PCR in this study are listed in Supporting Information Table S2. Subsequently, we analyzed a colorectal cancer tissue microarray ($n = 160$) and found that TGF-β1 expression was significantly elevated in tumor samples compared with adjacent tissues, particularly in those from pMMR patients (Fig. 1E and F, Fig. S2B). Moreover, high TGF-β1 expression was consistently associated with poor prognosis across colorectal cancer and pMMR colorectal cancer (Fig. 1G, Fig. S2C). Given the widely recognized role of TGF-β1 as a pleiotropic suppressor of antitumor immunity, we hypothesized that knocking out tumor-derived TGF-β1 could enhance the immunogenicity of tumor cell vaccines. Accordingly, TGF-β1 knockout (KO) tumor cells were generated using CRISPR-Cas9 technology, with successful knockout confirmed by Western blot, and ELISA (Fig. 1H and I). Proliferation rates of TGF-β1 KO cells were comparable to wild-type controls *in vitro* and in nude mice (Fig. S2D−S2F), suggesting that knockout of TGF-β1 did not affect tumor cell growth. To further evaluate potential compensatory molecular changes following TGF-β1 knockout, quantitative PCR analysis showed that *Tgfb2* and *Tgfb3* were not upregulated and their expression levels remained unchanged (Supporting Information Fig. S3).

To assess whether knockout of tumor-derived TGF-β1 enhances immunogenicity, we subcutaneously injected TGF-β1 knockout (KO) tumor cells into immunocompetent mice. Strikingly, CT26 TGF-β1 KO cells were completely rejected within one week in BALB/c mice (Fig. 1J), and MC38 TGF-β1 KO cells were similarly rejected in C57BL/6 mice (Fig. 1K). To evaluate whether this rejection conferred durable immunological memory, tumor-free mice from both models were rechallenged with syngeneic wild-type tumor cells. All mice previously exposed to TGF-β1 KO cells resisted tumor growth and remained tumor-free (Fig. 1L and M). These findings demonstrate that knockout of tumor-derived TGF-β1 substantially enhances tumor immunogenicity, enabling effective immune recognition and long-term antitumor protection *in vivo*.

Based on these results, we generated an inactivated whole-tumor cell vaccine using TGF-β1-knockout cells (referred to as Tβ1KO Vac). Flow cytometry of the vaccine administration site

therapeutic vaccination ($n = 6$). (F) Schematic of the CT26 lung metastasis model established by tail vein injection. Lungs were harvested at the endpoint for metastatic nodule analysis. (G, H) Representative images (G) and quantification (H) of lung metastatic nodules following treatment in the CT26 metastasis model ($n = 5$). (I) Schematic of the AOM/DSS-induced colitis-associated cancer (CAC) model. (J) Representative endoscopic images of the distal colon before (left) and after (right) therapeutic vaccination in the AOM/DSS model. (K) Representative macroscopic images of the distal colon at the endpoint. (L) Quantification of total tumor area in the distal colon at the endpoint ($n = 12$). Statistical significance was determined using two-way ANOVA for tumor growth curves, one-way ANOVA with Tukey's *post hoc* test for flow cytometry and tumor burden, and the log-rank (Mantel-Cox) test for survival analysis. Data are shown as mean ± SD. $*P < 0.05$, $**P < 0.01$, $***P < 0.001$, $****P < 0.0001$ *vs.* indicated; ns, not significant.

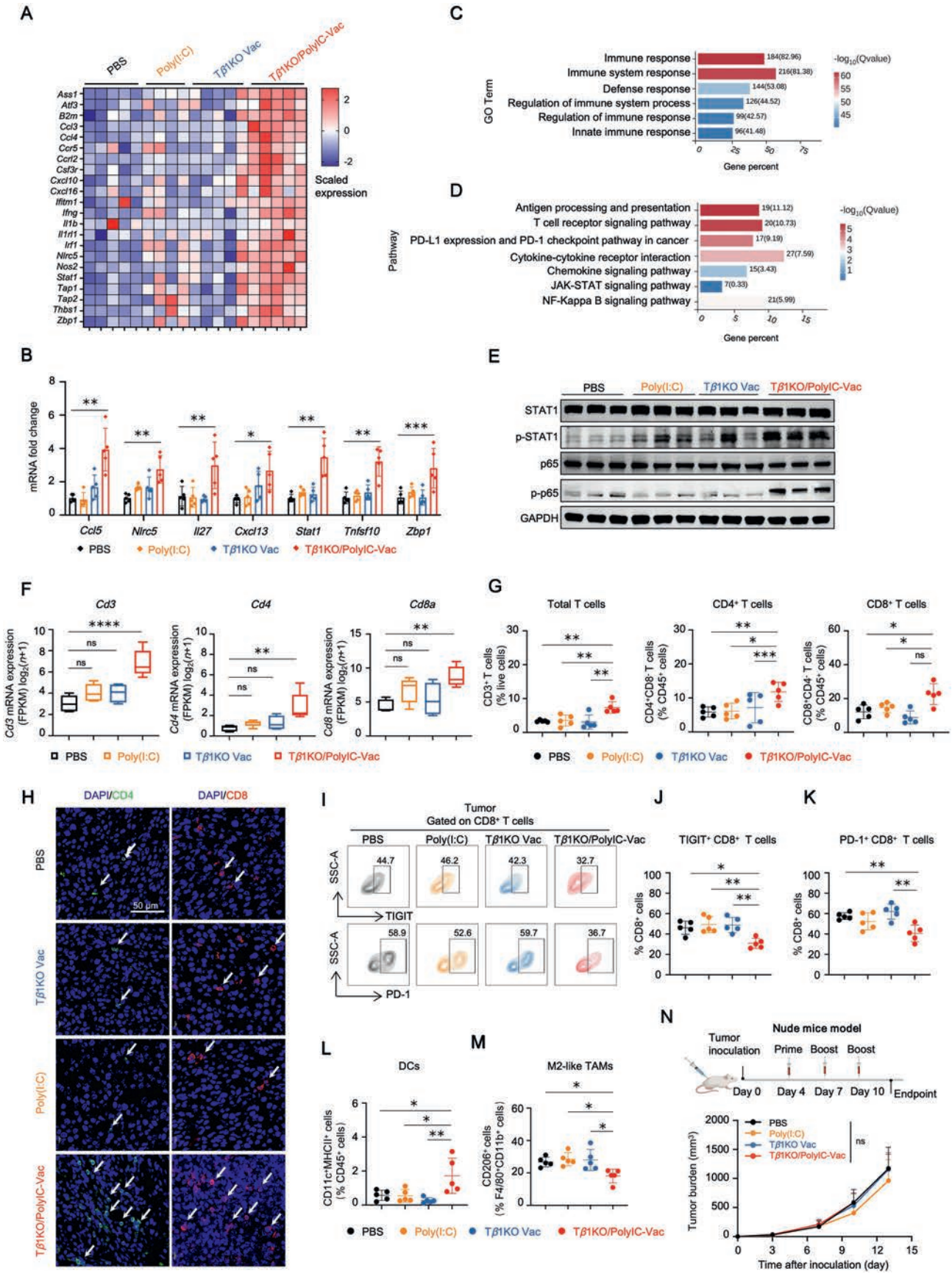

Figure 3 Tβ1KO/PolyIC-Vac treatment reprograms the pMMR tumor immune microenvironment. (A) Heatmap of differentially expressed immune-related genes in tumors after treatment, based on RNA-seq. (B) Quantitative PCR (qPCR) analysis of immune-related genes in tumor-

revealed reduced MDSC accumulation and increased dendritic cell and M1-like macrophages infiltration (Fig. 1N). These results suggest that knockout of tumor-derived TGF-β1 reprograms the local immune landscape, alleviating immunosuppression and enhancing immune activation.

3.3. Tβ1KO/PolyIC-Vac significantly suppresses distal tumor growth and extends survival in subcutaneous models

We next evaluated the therapeutic efficacy of the vaccine following the treatment schedule outlined in Fig. 1A. However, Tβ1KO Vac alone showed limited therapeutic benefit in pMMR tumors (Fig. 2A and B), indicating that relief of immunosuppression is insufficient without additional immune priming. Therefore, we combined Tβ1KO Vac with the immunostimulatory adjuvant Poly(I:C), for which we also explored the optimal dosing, to generate Tβ1KO/PolyIC-Vac (Supporting Information Fig. S4A). The addition of Poly(I:C) significantly enhanced the therapeutic efficacy of Tβ1KO Vac, resulting in complete tumor regression in 30% of mice and a marked extension of overall survival (Fig. 2A and B, Fig. S4B). Immune profiling at the vaccine administration site revealed increased infiltration of T cells, dendritic cells (DCs), and M1-like macrophages, with reduced MDSCs in the Tβ1KO/PolyIC-Vac group (Fig. 2C). In addition, consistent suppression of distal tumor growth was observed in MC38 and B16 tumor models (Fig. 2D and E).

3.4. Biosafety evaluation of Tβ1KO/PolyIC-Vac

Given the importance of safety in clinical immunotherapy, we first confirmed that irradiated tumor cells used for vaccine preparation exhibited markedly impaired proliferation *in vitro* and completely inhibited tumor formation *in vivo* (Supporting Information Fig. S4C and S4D). Furthermore, following subcutaneous vaccination, we evaluated the systemic toxicity of Tβ1KO/PolyIC-Vac. No significant alterations were detected in liver function markers (ALB, ALT, AST) or kidney function markers (CREA, UA, UREA) (Fig. S4E and S4F). In addition, histopathological examination of major organs, including the heart, liver, spleen, lung, and kidney, revealed no abnormalities (Fig. S4G).

3.5. Tβ1KO/PolyIC-Vac effectively suppresses distant pulmonary metastases

Effective control of metastatic lesions remains a major challenge in cancer immunotherapy. To assess whether Tβ1KO/PolyIC-Vac could be effective against distant metastases, a pulmonary micrometastasis model was established by intravenously injecting CT26 tumor cells into mice (Fig. 2F). Treatment with Tβ1KO/PolyIC-Vac significantly inhibited tumor growth in the lungs and reduced metastatic burden (Fig. 2G and H), demonstrating its capacity to control distant tumor metastases.

3.6. Tβ1KO/PolyIC-Vac effectively suppresses the progression of spontaneous pMMR-type colorectal cancer

To evaluate the therapeutic potential of Tβ1KO/PolyIC-Vac in spontaneous pMMR-type colorectal cancer, we established an AOM/DSS-induced colitis-associated cancer model (Fig. 2I). Western blot analysis confirmed that the primary tumors exhibited a pMMR phenotype (Supporting Information Fig. S5). Upon detection of epithelial dysplasia, subcutaneous vaccination was administered. Colonoscopy revealed extensive distal colonic tumors with mucosal hyperemia and edema in the PBS and Poly(I:C) groups. Tβ1KO Vac partially reduced tumor burden, but lesions remained prominent. In contrast, Tβ1KO/PolyIC-Vac preserved mucosal architecture and markedly reduced tumor size with well-defined boundaries (Fig. 2J and K). Histopathological analysis confirmed a significant reduction in tumor area in the distal colon compared to the PBS group (Fig. 2L). These findings suggest that Tβ1KO/PolyIC-Vac effectively suppresses inflammation-driven colorectal cancer progression and highlight its potential as a universal therapeutic strategy for pMMR-type tumors.

In summary, Tβ1KO/PolyIC-Vac achieved durable tumor control across subcutaneous, metastatic, and spontaneous pMMR tumor models, establishing its potential as a broadly applicable and clinically translatable immunotherapy.

3.7. Tβ1KO/PolyIC-Vac treatment reprograms the tumor microenvironment

To elucidate the mechanism underlying the antitumor effects of the Tβ1KO/PolyIC-Vac, RNA-seq was performed on tumor tissues following treatment. Differential gene expression analysis revealed significant upregulation of key chemokines (*Ccl3*, *Ccl4*, and *Ccl5*) and antigen presentation-related genes (*B2m, Nlrc5*) in the Tβ1KO/PolyIC-Vac group (Fig. 3A and B). Gene Ontology (GO) enrichment analysis showed enrichment of immune-related processes such as "immune response" (Fig. 3C), and KEGG analysis indicated activation of pathways including "antigen processing and presentation", "JAK−STAT signaling", and "NF-κB signaling" (Fig. 3D). Moreover, Western blot analysis confirmed activation of the NF-κB and JAK-STAT1 pathways (Fig. 3E). Together, these results demonstrate that Tβ1KO/PolyIC-Vac treatment induces a pro-inflammatory tumor microenvironment, thereby inhibiting the growth of distal pMMR tumors.

derived RNA samples ($n = 5$). (C) Gene Ontology (GO) enrichment analysis of upregulated genes identified by RNA-seq. (D) Kyoto Encyclopedia of Genes and Genomes (KEGG) pathway analysis showing enrichment of immune-related signaling pathways. (E) Western blot analysis of tumor lysates for NF-κB (p65, phospho-p65) and JAK−STAT1 (STAT1, phospho-STAT1). GAPDH served as a loading control. (F) RNA-seq-based expression of *Cd3*, *Cd4*, and *Cd8* genes across treatment groups. Data are shown as FPKM values $\log_2(n+1)$. (G) Flow cytometric analysis of tumor-infiltrating $CD3^+$, $CD4^+$, and $CD8^+$ T cells ($n = 5$). (H) Representative immunofluorescence images of $CD4^+$ (green) and $CD8^+$ (red) T cells in CT26 tumors. Nuclei were counterstained with DAPI (blue). Scale bar, 50 μm. (I−K) Flow cytometric analysis of PD-1 and TIGIT expression on $CD8^+$ T cells isolated from tumors ($n = 5$). (L, M) Flow cytometric analysis of tumor-infiltrating dendritic cells ($CD11c^+MHCII^+$) and M2-like tumor-associated macrophages ($CD11b^+F4/80^+CD206^+$) ($n = 5$). (N) Tumor growth curves in nude mice treated with PBS (black), Poly(I:C) (orange), Tβ1KO Vac (blue), or Tβ1KO/PolyIC-Vac (red) ($n = 8$). Statistical significance was determined using one-way ANOVA with Tukey's *post hoc* test for multiple group comparisons and two-way ANOVA for tumor growth curves. Data are shown as mean ± SD. $^*P < 0.05$, $^{**}P < 0.01$, $^{***}P < 0.001$, $^{****}P < 0.0001$ *vs.* indicated; ns, not significant.

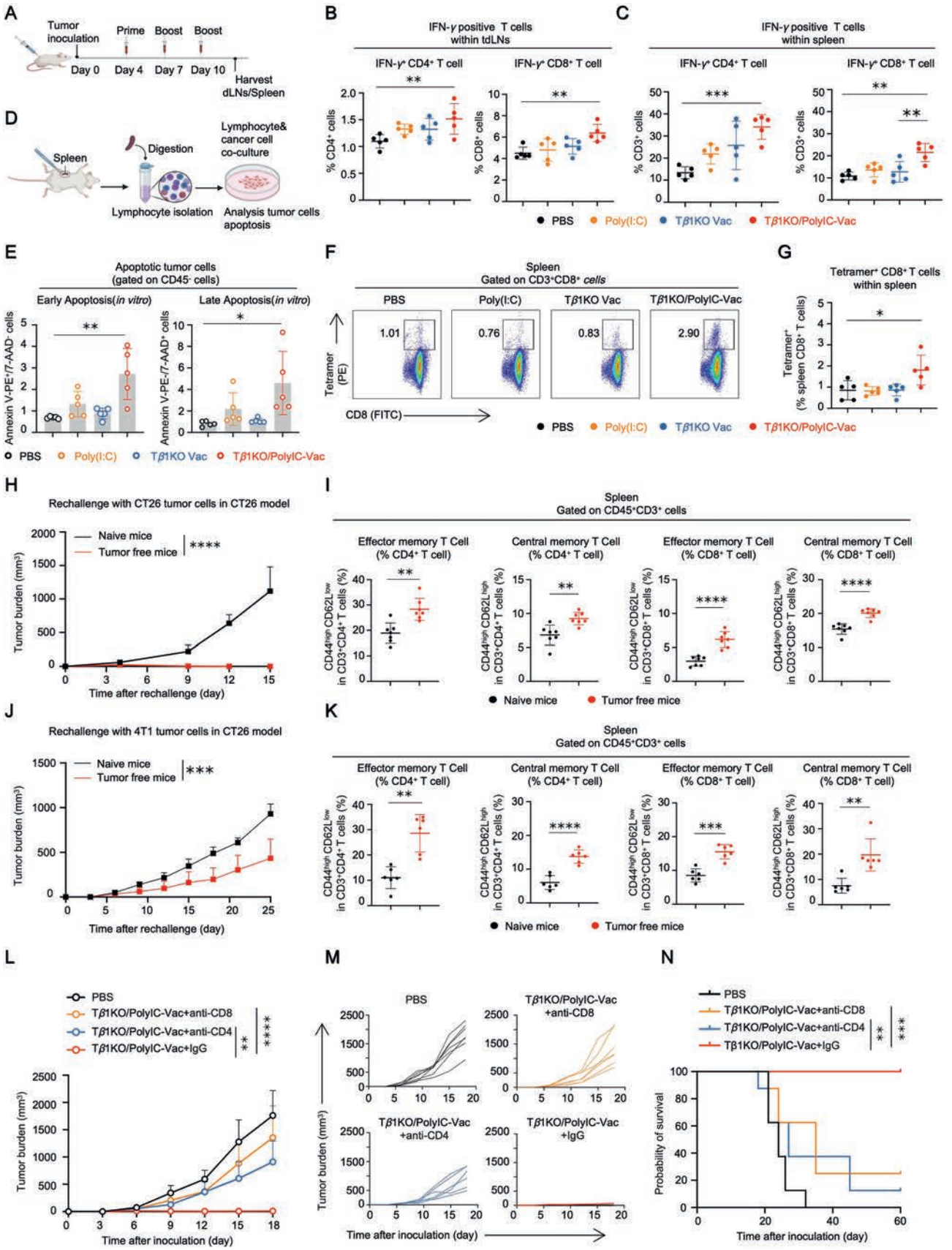

Figure 4 Therapeutic administration of Tβ1KO/PolyIC-Vac elicits a durable and cross-protective T cell−dependent antitumor immune response. (A) Experimental timeline showing tumor inoculation, vaccination schedule, and tissue harvest. CT26 tumor-bearing mice were

To further assess how Tβ1KO/PolyIC-Vac reshapes the immune landscape of distal tumors, RNA-seq data were analyzed for immune cell marker gene expression. Compared to the other three treatment groups, expression levels of *Cd3*, *Cd4*, and *Cd8a* were significantly elevated following Tβ1KO/PolyIC-Vac (Fig. 3F). Flow cytometric analysis confirmed a marked increase in $CD3^+$, $CD4^+$, and $CD8^+$ T cell populations within the tumor following vaccination (Fig. 3G), which was further validated by immunofluorescence staining (Fig. 3H). In addition, Tβ1KO/PolyIC-Vac decreased the proportion of $TIGIT^+$ and PD-1^+ tumor-infiltrating T cells, indicating enhanced T cell functionality within the tumor (Fig. 3I−K). Furthermore, Tβ1KO/PolyIC-Vac significantly increased intratumoral dendritic cell infiltration and was associated with a reduction in M2-like tumor-associated macrophages (Fig. 3L and M), supporting a shift toward a more immunostimulatory microenvironment. Collectively, these results demonstrate that Tβ1KO/PolyIC-Vac reprograms the tumor immune microenvironment.

3.8. The antitumor effect of Tβ1KO/PolyIC-Vac depends on host endogenous T cells

To evaluate whether the therapeutic efficacy of Tβ1KO/PolyIC-Vac depends on T cells, vaccination experiments were performed in immunodeficient nude mice lacking functional T lymphocytes. The results showed that the antitumor effect observed in immunocompetent models was completely abolished in these mice (Fig. 3N, Supporting Information Fig. S6). These findings indicate that the antitumor effect of Tβ1KO/PolyIC-Vac is likely driven by host T cells, with a predominant role for antigen-specific adaptive immunity over innate mechanisms.

3.9. Tβ1KO/PolyIC-Vac activates systemic, antigen-specific T cell responses

To investigate systemic immunity induced by Tβ1KO/PolyIC-Vac, tumor-draining lymph nodes and spleens were analyzed (Fig. 4A). Flow cytometry showed significantly increased frequencies of IFN-γ^+CD8^+ and IFN-γ^+CD4^+ T cells in both lymph nodes and spleens following Tβ1KO/PolyIC-Vac treatment (Fig. 4B and C). To assess the cytotoxic capacity of splenic lymphocytes, splenocytes were co-cultured with tumor cells *in vitro* (Fig. 4D). The results revealed that splenic lymphocytes from the Tβ1KO/PolyIC-Vac group significantly promoted tumor cell apoptosis compared to the control group (Fig. 4E). Moreover, the frequency of antigen-specific $Tetramer^+CD8^+$ T cells was markedly higher in the Tβ1KO/PolyIC-Vac group than other treatment groups (Fig. 4F and G). Together, these results demonstrate that Tβ1KO/PolyIC-Vac elicits robust systemic, antigen-specific T cell responses capable of mediating tumor clearance at distant sites.

3.10. Tβ1KO/PolyIC-Vac induces long-term, cross-protective immune memory

To assess whether Tβ1KO/PolyIC-Vac induces durable antitumor memory, tumor-free mice were rechallenged 60 Days after clearance with CT26 cells. All previously vaccinated mice resisted tumor rechallenge, indicating the establishment of long-lasting antitumor immune protection (Fig. 4H). To evaluate the breadth of memory responses, heterologous 4T1 cells were implanted in the same cohort, and mice also showed significant resistance (Fig. 4J), demonstrating cross-protective memory induced by Tβ1KO/PolyIC-Vac. Following rechallenge, T cell subsets in spleen were analyzed, revealing significantly increased $CD8^+$ effector memory ($CD44^+CD62L^-$) and central memory ($CD44^+CD62L^+$) T cells in the Tβ1KO/PolyIC-Vac group (Fig. 4I−K). These results indicate that Tβ1KO/PolyIC-Vac establishes robust and durable antitumor immune memory with cross-protective potential.

To determine which T cell subsets are required for protection, $CD4^+$ or $CD8^+$ T cells were selectively depleted after vaccination and mice were subsequently inoculated with tumors (Supporting Information Fig. S7). Depletion of either subset reduced vaccine efficacy (Fig. 4L−N), indicating that both $CD4^+$ and $CD8^+$ T cells are essential for sustaining durable antitumor immunity.

3.11. Tβ1KO/PolyIC-Vac promotes plasma cell recruitment and $CD8^+$ T cell activation in lymph nodes

To further elucidate how Tβ1KO/PolyIC-Vac stimulates adaptive immunity, single-cell RNA sequencing was performed on vaccine-draining lymph nodes collected from the immunized side following subcutaneous administration. Unsupervised clustering identified 15 distinct immune cell clusters (Fig. 5A, Supporting Information Fig. S8A). Compared to the WT Vac group, the Tβ1KO Vac group exhibited a decrease in naïve T cells, $CD4^+$ T cells, and regulatory T cells (Tregs), alongside an increase in B cells and plasma cells. Notably, the addition of Poly(I:C) led to a further reduction in naïve T and Treg proportions, alongside a significant increase in the frequency of $CD4^+$ T cells (Fig. 5B). These changes indicate enhanced immune activation in lymph

vaccinated, and tumor-draining lymph nodes (TdLNs) and spleens were collected 3 Days after the final vaccination. (B, C) Flow cytometric analysis of IFN-γ^+CD8^+ and IFN-γ^+CD4^+ T cells in TdLNs (B) and spleens (C) ($n = 5$). (D) Schematic of the *in vitro* co-culture assay. Splenic lymphocytes were isolated from vaccinated mice, co-cultured with tumor cells, and tumor cell apoptosis was subsequently evaluated. (E) Flow cytometric analysis of tumor cell apoptosis after co-culture with splenic lymphocytes ($n = 5$). (F) Representative flow cytometry plots showing tumor antigen-specific $tetramer^+$ $CD8^+$ T cells in spleens. (G) Flow cytometric analysis of $tetramer^+$ $CD8^+$ T cells in spleens across treatment groups ($n = 5$). (H) Tumor growth curves of previously tumor-free mice rechallenged with CT26 cells (red) compared with naïve controls (black) ($n = 7$). (I) Flow cytometric analysis of effector memory ($CD44^+CD62L^-$) and central memory ($CD44^+CD62L^+$) subsets within $CD4^+$ and $CD8^+$ T cells in spleens of rechallenged mice ($n = 7$). (J) Tumor growth curves of previously tumor-free mice rechallenged with 4T1 cells (red) compared with naïve controls (black) ($n = 7$). (K) Flow cytometric analysis of effector memory and central memory subsets within $CD4^+$ and $CD8^+$ T cells in spleens of mice rechallenged with 4T1 cells ($n = 6$). (L) Tumor growth curves in vaccinated mice with or without $CD4^+$ or $CD8^+$ T cell depletion ($n = 7$). (M) Individual tumor growth curves for each mouse in the four treatment groups. (N) Kaplan−Meier survival curves of mice from each treatment group. Statistical significance was determined using one-way ANOVA with Tukey's *post hoc* test for multiple group comparisons, two-way ANOVA for tumor growth curves, and log-rank (Mantel-Cox) test for survival analysis. Data are shown as mean ± SD. $*P < 0.05$, $**P < 0.01$, $***P < 0.001$, $****P < 0.0001$ *vs.* indicated.

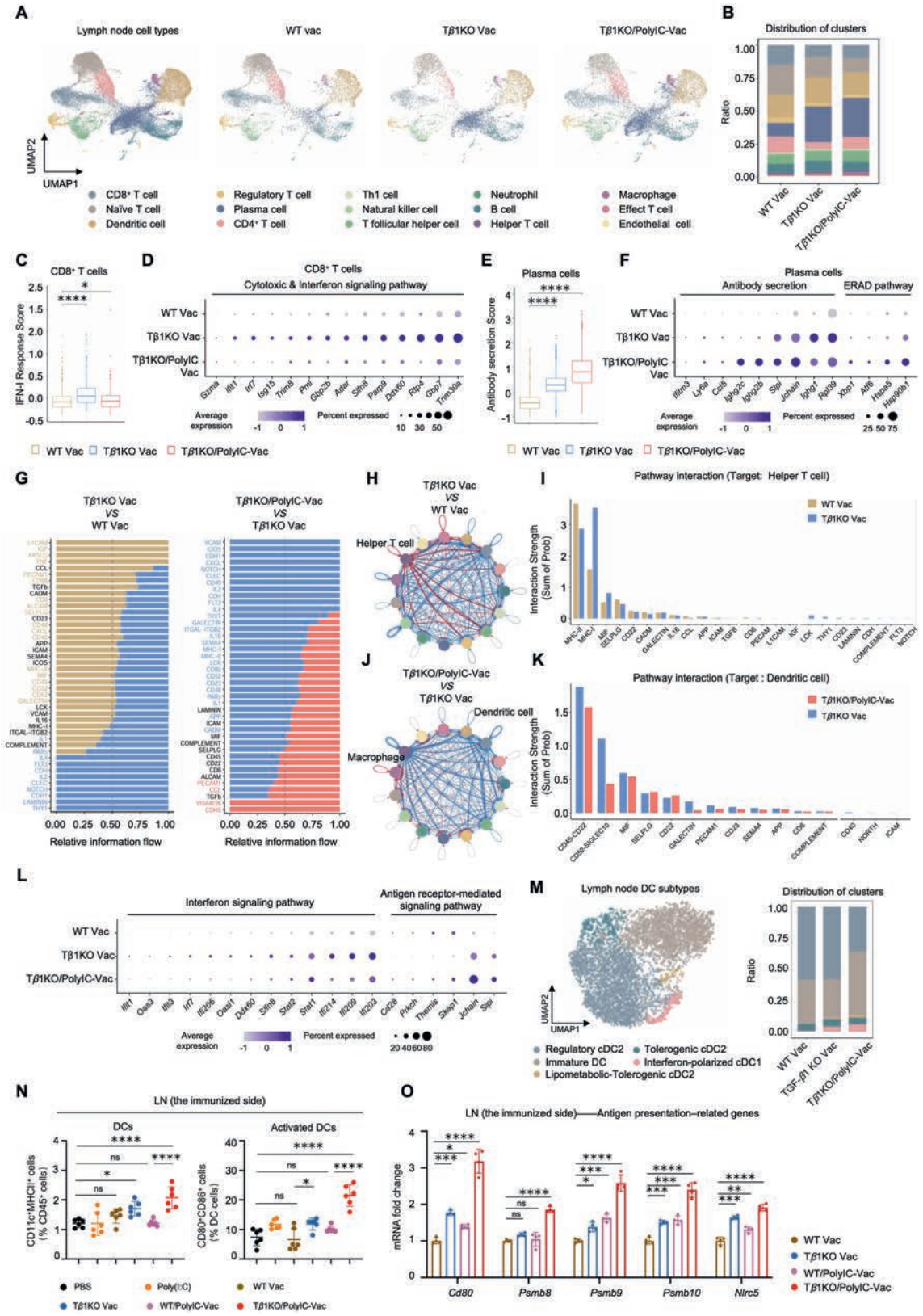

Figure 5 Tβ1KO/PolyIC-Vac vaccination promotes cDC1 interferon polarization in vaccine-draining lymph nodes, thereby initiating tumor-specific immune priming. (A) Uniform Manifold Approximation and Projection (UMAP) of lymph node cell subsets at vaccination sites. (B) Proportional distribution of major immune cell types in WT Vac, Tβ1KO Vac, and Tβ1KO/PolyIC-Vac groups. (C) Module scores for type I interferon response genes in $CD8^+$ T cells, calculated using Seurat. (D) Module scores for antibody secretion genes in plasma cells. (E) Bubble plot showing expression of cytotoxicity-related and interferon-stimulated genes in $CD8^+$ T cells across treatment groups. (F) Bubble plot showing

nodes following subcutaneous administration of Tβ1KO/PolyIC-Vac.

To evaluate CD8$^+$ T cell function, GSEA revealed enrichment in immune response pathways in the Tβ1KO Vac group (Fig. S8B−S8D), with elevated expression of cytotoxic and type I interferon-responsive genes (*Gzma, Irf7, Isg15, Ifit1*) (Fig. 5D). Single-cell IFN-I signature score confirmed enhanced CD8$^+$ T cell activation in both Tβ1KO Vac and Tβ1KO/PolyIC-Vac groups (Fig. 5C). Collectively, these results demonstrate that Tβ1KO/PolyIC-Vac enhances CD8$^+$ T cell effector function, thereby augmenting adaptive immunity in vaccine-draining lymph nodes.

To evaluate the humoral immune response induced by vaccination, plasma cell function was analyzed in the vaccine-draining lymph nodes. Gene Ontology analysis revealed that upregulated genes in the Tβ1KO Vac group were enriched in humoral immunity pathways, with increased expression of antibody-associated genes such as *Jchain* and *Ighg1* (Supporting Information Fig. S9A and S9C). The addition of Poly(I:C) further activated ER stress pathways and upregulated immunoglobulin genes, including *Ighg2b* and *Ighgc* (Fig. S9B and S9D). Antibody secretion scores confirmed enhanced plasma cell functionality, particularly in the Tβ1KO/PolyIC-Vac group (Fig. 5E and F). These findings indicate that Tβ1KO/PolyIC-Vac promotes plasma cell recruitment and enhances antibody secretion in the draining lymph nodes.

3.12. Tβ1KO/PolyIC-Vac promotes interferon-polarized cDC1 activation and reshapes lymph node immune communication

To investigate how Tβ1KO/PolyIC-Vac modulates antigen presentation, CellChat analysis was performed to infer cell-cell communication networks within vaccine-draining lymph nodes. The results revealed distinct intercellular signaling patterns across the different vaccine groups (Supporting Information Fig. S10A and S10B). Compared to the WT Vac group, the Tβ1KO Vac treatment significantly enhanced signaling pathways mediated by IL-1, IL-2, IL-4, and CDH1 (Fig. 5G), with a notable increase in signals received by helper T cells (Fig. 5H). This was accompanied by enhanced MHC class I signaling and a reduction in MHC class II signaling (Fig. 5I), suggesting a shift toward cytotoxic T cell priming. The addition of Poly(I:C) further strengthened PECAM1, CCL, and VISFATIN-mediated signaling (Fig. 5G), with increased signal input into macrophages and a slight reduction in inter-DC communication (Fig. 5J). Further analysis revealed a marked increase in CD45−CD22 signaling received by macrophages (Supporting Information Fig. S11C). Additionally, inhibitory signals in DCs, such as CD45−CD22 and CD52−SIGLEC10, were significantly downregulated (Fig. 5K), suggesting that Tβ1KO/PolyIC-Vac alleviates local immune-suppression and enhances DC activation in the vaccine-draining lymph nodes.

To evaluate the impact of Tβ1KO/PolyIC-Vac on DC function, gene expression profiles in DCs were examined. In the Tβ1KO Vac group, genes related to MHC-I antigen presentation and type I interferon pathways (*e.g.*, *Ifit1*, *Oas3*, *Ifi206*) were significantly upregulated (Fig. 5L, Fig. S11A). Upon Poly(I:C) addition, expression of MHC-II antigen processing genes *Prkch* and *Skap1* was further elevated (Fig. 5L, Fig. S11B). Subtype analysis revealed an increased proportion of Interferon-polarized cDC1 cells with antigen-presenting and immune-activating potential, while the proportion of Regulatory cDC2 decreased in the Tβ1KO/PolyIC-Vac group (Fig. 5M, Fig. S11D and S11E).

To validate these findings, flow cytometry was used to assess the frequency and activation status of DCs in draining lymph nodes. Compared to the WT Vac group, the Tβ1KO/PolyIC-Vac group exhibited a significant increase in MHCII$^+$CD11C$^+$ DCs, along with elevated expression of activation markers CD80$^+$ and CD86$^+$ (Fig. 5N). In contrast, the combination of WT Vac and Poly(I:C) did not significantly enhance DC activation, suggesting that Poly(I:C) alone is insufficient to overcome TGF-β1-mediated immunosuppression and fully activate DCs. In summary, Tβ1KO/PolyIC-Vac promotes DC activation by relieving TGF-β1-mediated inhibitory signals, reshapes the local immune communication network in lymph nodes, and enhances antigen presentation, thereby potentiating antitumor adaptive immune responses.

To elucidate the molecular basis of the synergy between tumor cell−derived TGF-β1 deletion and Poly(I:C)−mediated immune activation, we analyzed immune-related gene expression in vaccine-draining lymph nodes and at the vaccination site following standard vaccination. In draining lymph nodes, Tβ1KO/PolyIC-Vac induced robust and coordinated upregulation of interferon signaling genes (*Ifit1*, *Ifitm3*, *Ifng*, *Irf7*, *Stat1*) (Supporting Information Fig. S12A) together with immunoproteasome components involved in antigen processing (*Psmb8*, *Psmb9*, *Psmb10*) (Fig. 5O). In contrast, Tβ1KO or Poly(I:C) alone elicited only modest and selective transcriptional changes (Fig. 5O; Fig. S12A). Consistent with these findings, Western blot analysis revealed the highest levels of STAT1 phosphorylation and PSMB9/PSMB10 expression in the Tβ1KO/PolyIC-Vac group (Fig. S12B).

At the vaccination site, Tβ1KO/PolyIC-Vac induced the strongest interferon response (Fig. S12C). In contrast, TGF-β1 deletion significantly reduced the expression of multiple immunosuppressive factors, whereas Poly(I:C) alone failed to

expression of antibody secretion and ER-associated degradation (ERAD) pathway genes in plasma cells. (G) CellChat analysis ranking signaling pathways by differential information flow. Left: Tβ1KO Vac *versus* WT Vac. Right: Tβ1KO/PolyIC-Vac *versus* Tβ1KO Vac. (H) Comparison of ligand-receptor interactions between immune cell subsets in Tβ1KO Vac *versus* WT Vac groups. Edge width represents interaction strength. Red edges indicate interactions enhanced in Tβ1KO Vac relative to WT Vac; blue edges indicate reduced interactions. (I) Differentially expressed ligand-receptor pairs with helper T cells as receptors in Tβ1KO Vac *versus* WT Vac groups. (J) Comparison of ligand-receptor interactions between immune cell subsets in Tβ1KO/PolyIC-Vac *versus* Tβ1KO Vac groups. (K) Differentially expressed ligand−receptor pairs with dendritic cells as receptors in Tβ1KO/PolyIC-Vac relative to Tβ1KO Vac. (L) Bubble plot showing expression of interferon signaling and antigen receptor-mediated signaling pathway genes in plasma cells across treatment groups. (M) UMAP of dendritic cell (DC) subclusters in draining lymph nodes and bar graph showing the proportion of each DC subset. (N) Flow cytometric analysis of MHCII$^+$CD11c$^+$ DCs and expression of activation markers CD80$^+$ and CD86$^+$ in vaccine-draining lymph nodes. (O) Quantitative PCR analysis of antigen presentation−related genes (*Cd80*, *Psmb8*, *Psmb9*, *Psmb10*, and *Nlrc5*) in vaccine-draining lymph nodes on the immunized side. Gene expression levels are presented as mRNA fold change relative to the WT vac group. Statistical significance was determined using one-way ANOVA with Tukey's *post hoc* test for multiple comparisons. Data are shown as mean ± SD. *$P < 0.05$, **$P < 0.01$, ***$P < 0.001$, ****$P < 0.0001$ *vs*. indicated; ns, not significant.

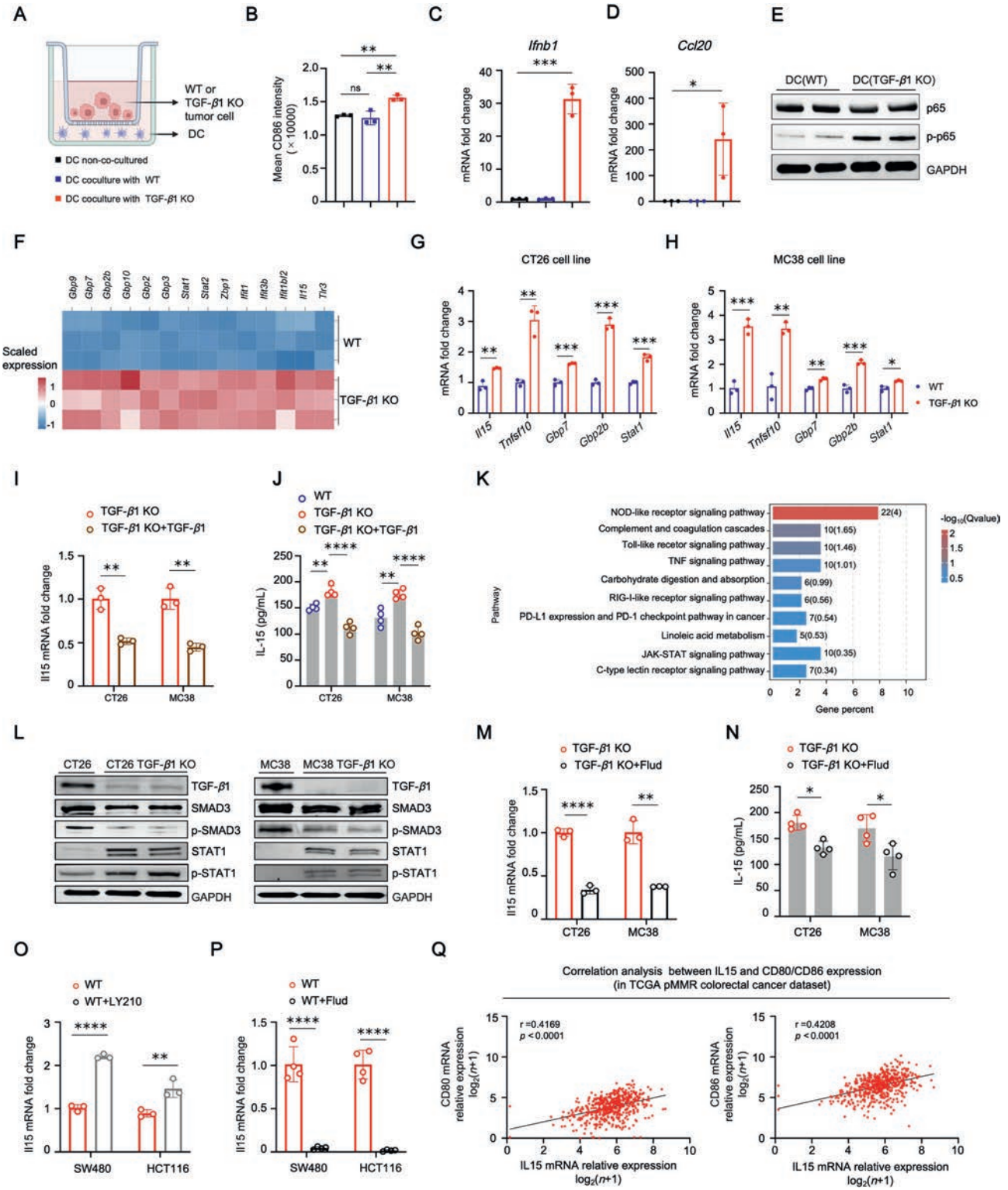

Figure 6 Knockout of tumor-derived TGF-β1 activates tumor-intrinsic STAT1−IL-15 signaling to promote dendritic cell activation. (A) Schematic of the transwell co-culture system. Tumor cells (WT or TGF-β1 KO) were seeded in the upper chamber, and DC2.4 cells were cultured in the lower chamber. After co-culture, DCs were collected for analysis of maturation and activation. (B) Mean fluorescence intensity (MFI) of CD86 on DCs following co-culture with WT or TGF-β1 KO tumor cells ($n = 3$). (C, D) mRNA expression of *Ifnb1* (C) and *Ccl20* (D) in DCs after co-culture ($n = 3$). (E) Western blot analysis of NF-κB (p65, phospho-p65) in DCs co-cultured with WT or TGF-β1 KO tumor cells. GAPDH served as a loading control. (F) Heatmap of upregulated immune-related genes in TGF-β1 KO tumor cells based on RNA-seq. (G, H) mRNA expression of *Il15* and related genes (*Gbp2b*, *Tnfsf10*, *Stat1*, and *Gbp7*) in CT26 and MC38 cells ($n = 3$). (I) Quantitative PCR analysis of Il15 mRNA levels in tumor cells with or without exogenous TGF-β1 (2 ng/mL) ($n = 3$). (J) ELISA of IL-15 protein levels in culture supernatants

effectively suppress these signals (Fig. S12D). Collectively, these data demonstrate that relief of immunosuppression by TGF-β1 knockout and immune activation by Poly(I:C) are both required for effective activation of interferon signaling and antigen processing programs.

3.13. Knockout of tumor-derived TGF-β1 activates tumor-intrinsic STAT1−IL-15 signaling to promote dendritic cell activation

To investigate whether knockout of tumor-derived TGF-β1 directly promotes dendritic cell (DC) activation, tumor cell lysates were incubated with DC2.4 cells (Supporting Information Fig. S13A). Lysates from TGF-β1 knockout (KO) cells significantly increased CD86 mean fluorescence intensity (MFI) compared with wild-type (WT) controls (Fig. S13B), indicating enhanced DC activation. To further assess whether TGF-β1 deficiency promotes DC maturation through paracrine mechanisms, a transwell co-culture system was established with tumor cells in the upper chamber and DC2.4 cells in the lower chamber (Fig. 6A). DCs co-cultured with TGF-β1 KO tumor cells displayed higher CD86 MFI than WT and non-co-cultured controls (Fig. 6B), along with elevated *Ifnb1* and *Ccl20* transcripts (Fig. 6C and D) and increased NF-κB p65 phosphorylation (Fig. 6E), indicating enhanced DC activation *via* tumor-derived soluble mediators.

To elucidate the underlying mechanisms, RNA-seq analysis was performed on WT and TGF-β1 KO tumor cells. Gene expression profiling, supported by experimental validation, revealed upregulation of inflammation-associated genes, including a marked increase in *Il15* (Fig. 6F−H). IL-15, a key driver of DC activation, was suppressed by exogenous TGF-β1, whereas ELISA confirmed enhanced secretion in KO cells that was reversed upon TGF-β1 reintroduction (Fig. 6I and J). To identify the signaling pathway driving IL-15 upregulation, KEGG analysis of TGF-β1 KO tumor cells showed enrichment of immune pathways such as "STAT signaling" and "Toll-like receptor signaling" (Fig. 6K). Western blot analysis further confirmed increased STAT1 phosphorylation together with reduced SMAD3 signaling in TGF-β1−knockout cells (Fig. 6L). Pharmacologic inhibition demonstrated that IL-15 induction depended on STAT1, as Fludarabine suppressed *Il15* expression while NF-κB blockade had no effect (Fig. 6M and N; Fig. S13C and S13D). Conversely, functional blockade of IL-15 or inhibition of STAT1 signaling markedly attenuated the ability of TGF-β1−deficient tumor cells to activate DCs, as evidenced by a significant reduction in CD86 MFI in DC2.4 cells (Supporting Information Fig. S14), providing direct functional confirmation of the STAT1−IL-15 axis in mediating DC activation. Together, these results establish that TGF-β1 knockout facilitates IL-15 upregulation *via* STAT1 activation, revealing a key mechanism by which tumor-derived TGF-β1 suppresses DC-stimulatory cytokine production.

3.14. The TGF-β1−IL-15−STAT1 axis is conserved in human tumor cells and correlates with DC activation

To determine whether TGF-β1 suppression also affects IL-15 expression in human tumor cells, colorectal cancer lines HCT116 and SW480 were treated with the TGF-β1 receptor inhibitor. QPCR analysis showed that blocking TGF-β1 signaling significantly increased IL15 mRNA expression (Fig. 6O) whereas Fludarabine, a STAT1 inhibitor, abrogated this effect (Fig. 6P), indicating that IL-15 expression is similarly regulated *via* the STAT1 signaling pathway in human colorectal cancer cells. Lastly, analysis of The Cancer Genome Atlas (TCGA) colorectal cancer dataset further revealed that IL15 expression positively correlated with DC co-stimulatory markers CD80 and CD86 (Fig. 6Q), suggesting a potential clinical relevance for targeting this pathway.

3.15. Tβ1KO/PolyIC-Vac overcomes the resistance of pMMR tumors to PD-1 blockade and induces durable antitumor immune memory

To overcome the limited efficacy of immune checkpoint blockade in poorly immunogenic tumors, we evaluated the combination of Tβ1KO/PolyIC-Vac and anti-PD-1 therapy in CT26 tumor model (Fig. 7A). Tβ1KO/PolyIC-Vac + anti-PD-1 significantly suppressed tumor growth and extended survival compared to either monotherapy (Fig. 7B−D). Complete tumor regression was achieved in 60% of mice receiving Tβ1KO/PolyIC-Vac + anti-PD-1 therapy, *versus* 30% with Tβ1KO/PolyIC-Vac alone and none in control groups (Fig. 7D). Upon rechallenge with CT26 cells all previously cured mice from the Tβ1KO/PolyIC-Vac + anti-PD-1 group rejected secondary CT26 implantation, indicating robust long-term immune protection (Fig. 7E). Flow cytometric analysis revealed elevated frequencies of $CD4^+$ and $CD8^+$ effector memory T cells ($CD44^+CD62L^-$) in these mice, supporting the establishment of durable immunological memory (Fig. 7F and G).

These data demonstrate that Tβ1KO/PolyIC-Vac enhances the efficacy of PD-1 blockade and primes lasting antitumor immunity in otherwise unresponsive tumors. This strategy may offer a promising approach for enhancing immunotherapeutic efficacy in microsatellite-stable colorectal cancer and other pMMR tumors.

4. Discussion

Colorectal cancer (CRC) is characterized by more than 85% of cases being mismatch repair−proficient (pMMR), a subtype

($n = 4$). (K) KEGG pathway enrichment analysis showing immune-related pathways upregulated in TGF-β1 KO tumor cells. (L) Western blot analysis of phosphorylated STAT1 (p-STAT1) and phosphorylated SMAD3 (p-SMAD3) in WT and TGF-β1 KO tumor cells. (M) qPCR analysis of Il15 expression in CT26 cells treated with 6 μmol/L Fludarabine and MC38 cells treated with 10 μmol/L Fludarabine ($n = 3$). (N) ELISA of IL-15 protein levels in CT26 cells treated with 6 μmol/L Fludarabine and MC38 cells treated with 10 μmol/L Fludarabine ($n = 4$). (O) qPCR analysis of IL15 mRNA in SW480 cells treated with 25 μmol/L LY2109761 (a TGF-β receptor inhibitor) and HCT116 cells treated with 15 μmol/L LY2109761, with WT controls ($n = 3$). (P) qPCR analysis of IL15 mRNA in SW480 cells treated with 15 μmol/L Fludarabine (a STAT1 phosphorylation inhibitor) and HCT116 cells treated with 10 μmol/L Fludarabine, with WT controls ($n = 4$). (Q) Correlation analysis of IL15 expression with CD80 and CD86 expression in the TCGA pMMR colorectal cancer dataset. Statistical significance was determined using one-way ANOVA with Tukey's *post hoc* test for multiple group comparisons and unpaired two-tailed Student's *t* test for two-group comparisons. Correlation analyses were performed using Pearson's correlation. Data are shown as mean ± SD. *$P < 0.05$, **$P < 0.01$, ***$P < 0.001$, ****$P < 0.0001$ *vs*. indicated; ns, not significant.

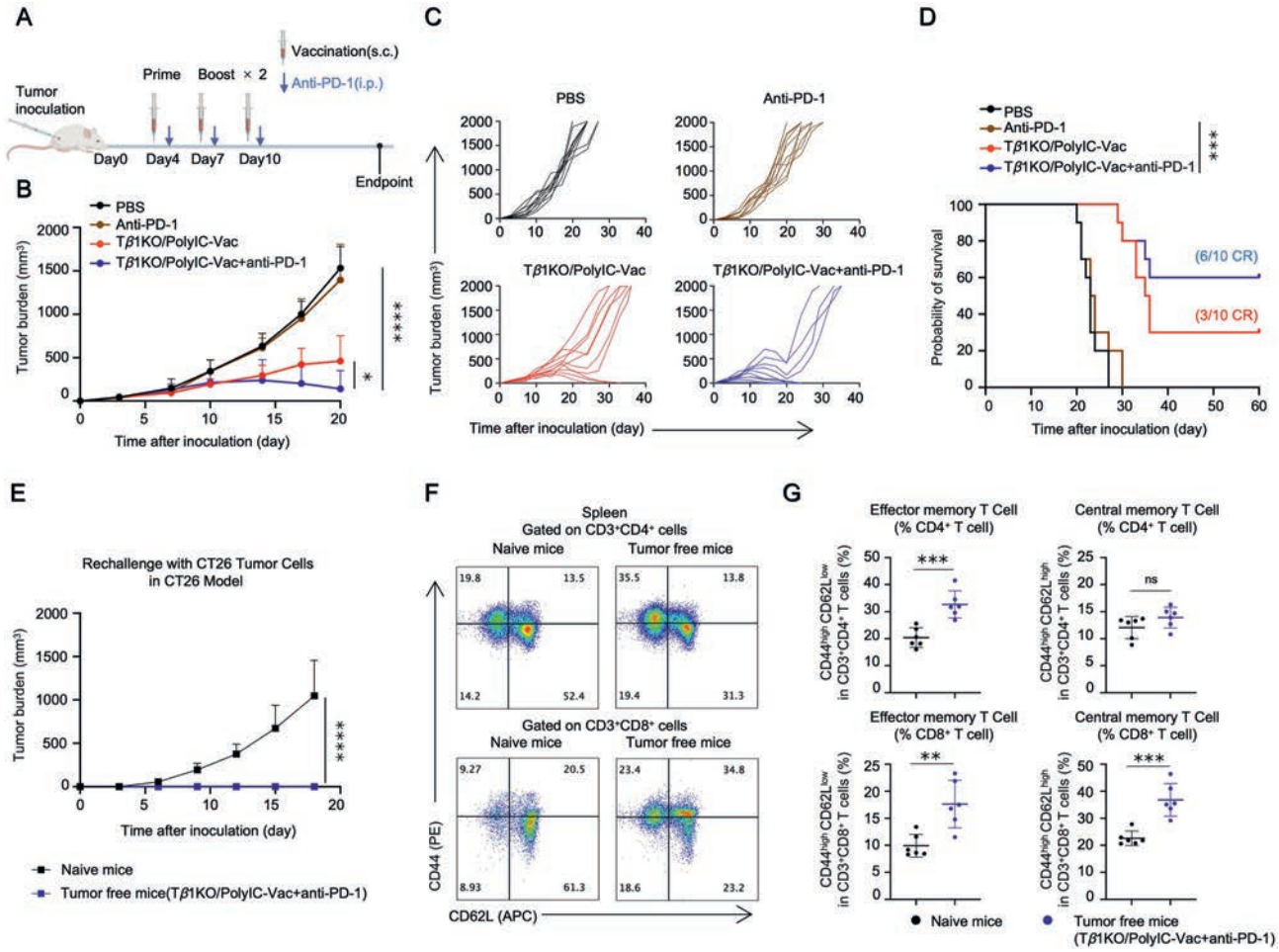

Figure 7 TB1KO/PolyIC-Vac overcomes the resistance of pMMR tumors to PD-1 blockade and induces durable antitumor immune memory. (A) Schematic of the treatment protocol. Mice bearing subcutaneous CT26 tumors were treated with TB1KO/PolyIC-Vac (s.c.) and anti-PD-1 antibody (i.p.) on Days 4, 7, and 10 post-tumor inoculation. (B) Tumor growth curves of mice treated with PBS (black), anti-PD-1 (orange), TB1KO/PolyIC-Vac (blue), or TB1KO/PolyIC-Vac + anti-PD-1 (red) ($n = 10$). (C) Individual tumor growth curves for each mouse in the four treatment groups. (D) Survival curves of mice in the indicated treatment groups. (E) Tumor growth curves after rechallenge with CT26 cells in previously tumor-free mice from the TB1KO/PolyIC-Vac + anti-PD-1 group ($n = 9$, blue) and in naive mice ($n = 9$, black). (F) Representative flow cytometry plots showing $CD44^+CD62L^-$ effector memory T cells and $CD44^+CD62L^+$ central memory T cells within $CD4^+$ and $CD8^+$ splenic T cells. (G) Flow cytometry analyse of effector memory ($CD44^+CD62L^-$) and central memory ($CD44^+CD62L^+$) T cells within $CD4^+$ and $CD8^+$ populations from tumor-free and naive mice ($n = 6$). Statistical significance was performed using two-way ANOVA with Bonferroni *post hoc* test for tumor growth curves and unpaired two-tailed Student's *t*-test for memory T cell analysis. Survival was analyzed using the log-rank (Mantel-Cox) test. Data are shown as mean ± SD. $^{**}P < 0.01$, $^{***}P < 0.001$, *vs.* indicated; ns, not significant.

classified as immunologically "cold" tumors[37]. Patients with advanced pMMR CRC typically exhibit weak antitumor immune responses and limited tumor-antigen recognition, resulting in poor clinical responses to immune-checkpoint inhibitors (ICIs) and chimeric antigen receptor (CAR)-T cell therapies[38]. Tumor vaccines have emerged as an alternative strategy capable of inducing tumor-specific immune responses and achieving effective tumor control[39]. However, the intrinsically low immunogenicity and substantial heterogeneity of pMMR tumors present major obstacles to the identification of tumor antigens with high immunogenicity and broad representation[40]. To overcome these limitations, we chose irradiated whole tumor cells as antigen-delivery vehicles. A key advantage of this format is the preservation of a comprehensive and native tumor antigen repertoire, including membrane-associated and conformational epitopes that are lost in lysates or extracellular vesicles[41]. In addition, irradiated tumor cells retain immunostimulatory programs induced by genetic editing or pharmacological modulation, enabling sustained immune activation[27,42,43].

Based on our preliminary data analyses and validation in clinical CRC specimens, we found that tumor-derived transforming growth factor-β1 (TGF-β1) is highly expressed in pMMR CRC and correlates with poor prognosis. Accordingly, we engineered pMMR tumor cells with CRISPR/Cas9-mediated knockout of TGF-β1, generating an antigen-delivery vehicle with relieved intrinsic immunosuppression. We found that TGF-β1 ablation reprogrammed the local immune microenvironment at the vaccination site. To further enhance immune activation, these engineered cells were combined with the TLR3 agonist Poly(I:C) to generate an engineered whole-tumor-cell vaccine, termed TB1KO/PolyIC-Vac. Subcutaneous administration of this vaccine markedly inhibited pMMR tumor growth and overcame PD-1 blockade

resistance, whereas unmodified pMMR tumor-cell vaccines failed to elicit therapeutic effects. Collectively, these findings demonstrate that Tβ1KO/PolyIC-Vac can effectively deliver a comprehensive tumor-antigen repertoire and restore immune recognition, thereby overcoming the immune-evasion of pMMR tumors.

Beyond shaping the tumor microenvironment, TGF-β1 also regulates tumor-intrinsic immunogenicity. It promotes epithelial-mesenchymal transition (EMT) *via* Smad-dependent upregulation of transcription factors such as Snail and Twist[44]. In hepatocellular carcinoma, TGF-β1 enhances CXCL12 and PD-L1 expression[34], further contributing to immune evasion. In this study, we unexpectedly found that knockout of TGF-β1 in pMMR tumor cells enhanced dendritic cell (DC) activation and induced IL-15 upregulation *via* STAT1 signaling. Importantly, this TGF-β1−STAT1−IL-15 axis was conserved in human colorectal cancer cell lines. These findings uncover a tumor-intrinsic immunosuppressive circuit mediated by TGF-β1, the disruption of which enhances the immunogenicity of tumor cell vaccines.

Optimizing antigen presentation and immune activation is central to tumor cell vaccine design. Whole-tumor cells facilitate broad antigen delivery by enabling efficient dendritic cell uptake through phagocytosis and antigen capture. Prior strategies have focused on engineering tumor cells to overexpress immunostimulatory cytokines such as GM-CSF, IL-7, or IL-21 to enhance immunogenicity[45,46]. Among these, GVAX demonstrated preclinical promise but showed limited efficacy in advanced solid tumors, particularly in "cold" cancers such as pancreatic adenocarcinoma. These findings suggest that enhancing immune stimulation alone is insufficient to overcome tumor-intrinsic immune suppression. To enhance the immunostimulatory capacity of TGF-β1−knockout tumor cells as antigen-delivery vehicles, we incorporated Poly(I:C), a TLR3 agonist that promotes DC activation and cross-presentation, thereby generating Tβ1KO/PolyIC-Vac. This approach couples the relief of tumor-intrinsic suppression with enhanced innate immune activation. Subsequent therapeutic studies demonstrated that this dual strategy, which concurrently relieves immune suppression and enhances immune activation, yields consistent antitumor efficacy across multiple tumor models. Mechanistically, TGF-β1 ablation promoted dendritic cell (DC) recruitment, and Poly(I:C) further enhanced DC activation and antigen presentation by disrupting the inhibitory CD52−SIGLEC10 axis. This strategy cooperatively primed adaptive immunity and suppressed distal tumor growth, highlighting that suppression relief and immune stimulation are both indispensable for effective vaccination.

With potential for clinical translation, both TCGA analyses and clinical studies indicate that tumor-derived TGF-β1 suppresses innate immune activation and antigen presentation in human cancers, consistent with the STAT1−IL-15 activation signature observed upon TGF-β1 knockout in our models. This concordance supports the biological rationale of targeting tumor-intrinsic TGF-β1 to enhance tumor immunogenicity in patients. Building on this mechanistic foundation, Tβ1KO/PolyIC-Vac represents an engineered vaccine platform that combines single-gene editing with innate immune stimulation to deliver a comprehensive repertoire of tumor antigens. In preclinical models, cell line−derived Tβ1KO/PolyIC-Vac significantly suppressed the growth of spontaneous orthotopic pMMR colorectal tumors. This efficacy is likely mediated, at least in part, by the presentation of shared tumor antigens, including tumor-associated antigens (TAAs), lineage-specific antigens (LSAs), and subsets of tumor-specific antigens, consistent with the broad antigen coverage of whole-cell vaccines[47−49]. Together, these results highlight the potential of Tβ1KO/PolyIC-Vac as a broadly applicable therapeutic strategy for pMMR/MSS tumors. In a clinical setting, however, interpatient tumor heterogeneity, antigenic evolution, and regulatory and manufacturing constraints associated with genetically engineered whole-cell products represent important challenges for translation. To address these issues, antigen relevance could be further optimized by profiling patient biopsy samples, for example, through DNA mutation−based antigen prediction, to identify individuals whose tumors exhibit high antigenic concordance with the vaccine source, thereby enabling biomarker-guided patient selection[50].

There are limitations to our study. Although the vaccine demonstrated efficacy across multiple murine pMMR tumor models, translation to human cancers will require validation in patient-derived xenografts, organoid systems, and ultimately clinical trials. In addition, while we identified the STAT1−IL-15 axis as a key pathway, other mechanisms may also contribute to the observed immune remodeling. This study was intended to establish the conceptual basis for combining the knockout of tumor-intrinsic immunosuppressive genes with an innate immune to stimulant, for which Poly(I:C) served as a representative adjuvant. Nonetheless, other innate immune stimulants with similar mechanistic attributes may also be applicable to this platform.

5. Conclusions

In summary, we developed Tβ1KO/PolyIC-Vac, an off-the-shelf whole-tumor-cell vaccine that simultaneously relieves immune suppression and enhances immune activation. These findings establish a mechanistic and antigen-delivery framework for developing universal tumor vaccines to overcome resistance in pMMR/MSS cancers.

Acknowledgments

This study was supported by the National Natural Science Foundation of China (No. 82573505, China); the Sichuan Science and Technology Program (No. 2025NSFTD0030, China; 2024NSFSC1931, China); and the 1·3·5 Project for Disciplines of Excellence, West China Hospital, Sichuan University (No. ZYGD23023, China).

Author contributions

Weixiao Yang, Zhexu Dong, Gang Shi and Hongxin Deng designed the research. Weixiao Yang and Zhexu Dong carried out the experiments and performed data analysis. Yushuang Ren, Lin Zhang, Jiaqi Han, Tian Tian, Yi Liu and Xiaolan Su participated in part of the experiments. Weixiao Yang and Zhexu Dong wrote the manuscript. Weixiao Yang, Zhexu Dong, Qi Xiong, Gang Shi and Hongxin Deng revised the manuscript. All of the authors have read and approved the final manuscript.

Conflicts of interest

The authors declare no conflicts of interest.

Appendix A. Supporting information

Supporting information to this article can be found online at https://doi.org/10.1016/j.apsb.2026.06.001.

References

1. Zhang M, Liu C, Tu J, Tang M, Ashrafizadeh M, Nabavi N, et al. Advances in cancer immunotherapy: historical perspectives, current developments, and future directions. *Mol Cancer* 2025;**24**:136.
2. Rafiq S, Hackett CS, Brentjens RJ. Engineering strategies to overcome the current roadblocks in CAR T cell therapy. *Nat Rev Clin Oncol* 2020;**17**:147−67.
3. Du B, Qin J, Lin B, Zhang J, Li D, Liu M. CAR-T therapy in solid tumors. *Cancer Cell* 2025;**43**:665−79.
4. Jin M, Fang J, Peng J, Wang X, Xing P, Jia K, et al. PD-1/PD-L1 immune checkpoint blockade in breast cancer: research insights and sensitization strategies. *Mol Cancer* 2024;**23**:266.
5. Kubli SP, Berger T, Araujo DV, Siu LL, Mak TW. Beyond immune checkpoint blockade: emerging immunological strategies. *Nat Rev Drug Discov* 2021;**20**:899−919.
6. Kalbasi A, Ribas A. Tumour-intrinsic resistance to immune checkpoint blockade. *Nat Rev Immunol* 2020;**20**:25−39.
7. Rousseau B, Patel M, Artz O, Vlachos G, Patel S, Hayatt O, et al. Induction of a mismatch repair deficient genotype by tailored chemical mutagenesis in experimental models of cancer. *Cancer Cell* 2025;**43**:1313−27.
8. Jin Z, Sinicrope FA. Mismatch Repair-deficient colorectal cancer: building on checkpoint blockade. *J Clin Oncol* 2022;**40**:2735−50.
9. Diaz Jr LA, Le DT. PD-1 blockade in tumors with mismatch-repair deficiency. *N Engl J Med* 2015;**373**:1979.
10. Ganesh K, Stadler ZK, Cercek A, Mendelsohn RB, Shia J, Segal NH, et al. Immunotherapy in colorectal cancer: rationale, challenges and potential. *Nat Rev Gastroenterol Hepatol* 2019;**16**:361−75.
11. Andre T, Tougeron D, Piessen G, de la Fouchardiere C, Louvet C, Adenis A, et al. Neoadjuvant nivolumab plus ipilimumab and adjuvant nivolumab in localized deficient mismatch repair/microsatellite instability-high gastric or esophagogastric junction adenocarcinoma: the GERCOR NEONIPIGA phase II study. *J Clin Oncol* 2023;**41**:255−65.
12. Westin SN, Moore K, Chon HS, Lee JY, Thomes Pepin J, Sundborg M, et al. Durvalumab plus carboplatin/paclitaxel followed by maintenance durvalumab with or without olaparib as first-line treatment for advanced endometrial cancer: the phase III DUO-E trial. *J Clin Oncol* 2024;**42**:283−99.
13. Eskander RN, Sill MW, Beffa L, Moore RG, Hope JM, Musa FB, et al. Pembrolizumab plus chemotherapy in advanced endometrial cancer. *N Engl J Med* 2023;**388**:2159−70.
14. van Wilpe S, Kloots ISH, Slootbeek PHJ, den Brok M, Westdorp H, Franken MD, et al. Ipilimumab with nivolumab in molecularly selected patients with castration-resistant prostate cancer: primary analysis of the phase II inspire trial. *Ann Oncol* 2024;**35**:1126−37.
15. Asaoka Y, Ijichi H, Koike K. PD-1 blockade in tumors with mismatch-repair deficiency. *N Engl J Med* 2015;**373**:1979.
16. Gajewski TF, Schreiber H, Fu YX. Innate and adaptive immune cells in the tumor microenvironment. *Nat Immunol* 2013;**14**:1014−22.
17. O'Donnell JS, Teng MWL, Smyth MJ. Cancer immunoediting and resistance to T cell-based immunotherapy. *Nat Rev Clin Oncol* 2019;**16**:151−67.
18. Peng K, Zhao X, Fu YX, Liang Y. Eliciting antitumor immunity via therapeutic cancer vaccines. *Cell Mol Immunol* 2025;**22**:840−68.
19. Lei W, Zhou K, Lei Y, Li Q, Zhu H. Cancer vaccines: platforms and current progress. *Mol Biomed* 2025;**6**:3.
20. Pail O, Lin MJ, Anagnostou T, Brown BD, Brody JD. Cancer vaccines and the future of immunotherapy. *Lancet* 2025;**406**:189−202.
21. Huber F, Bassani-Sternberg M. Defects in antigen processing and presentation: mechanisms, immune evasion and implications for cancer vaccine development. *Nat Rev Immunol* 2026;**26**:23−34.
22. Saxena M, van der Burg SH, Melief CJM, Bhardwaj N. Therapeutic cancer vaccines. *Nat Rev Cancer* 2021;**21**:360−78.
23. Carri I, Schwab E, Trivino JC, von Euw EM, Nielsen M, Mordoh J, et al. VACCIMEL, an allogeneic melanoma vaccine, efficiently triggers T cell immune responses against neoantigens and alloantigens, as well as against tumor-associated antigens. *Front Immunol* 2024;**15**:1496204.
24. Li N, Qin H, Zhu F, Ding H, Chen Y, Lin Y, et al. Potent prophylactic cancer vaccines harnessing surface antigens shared by tumour cells and induced pluripotent stem cells. *Nat Biomed Eng* 2025;**9**:215−33.
25. Gurung HR, Heidersbach AJ, Darwish M, Chan PPF, Li J, Beresini M, et al. Systematic discovery of neoepitope-HLA pairs for neoantigens shared among patients and tumor types. *Nat Biotechnol* 2024;**42**:1107−17.
26. Apavaloaei A, Zhao Q, Hesnard L, Cahuzac M, Durette C, Larouche JD, et al. Tumor antigens preferentially derive from unmutated genomic sequences in melanoma and non-small cell lung cancer. *Nat Cancer* 2025;**6**:1419−37.
27. Fang C, Mo F, Liu L, Du J, Luo M, Men K, et al. Oxidized mitochondrial DNA sensing by STING signaling promotes the antitumor effect of an irradiated immunogenic cancer cell vaccine. *Cell Mol Immunol* 2021;**18**:2211−23.
28. Wu AA, Bever KM, Ho WJ, Fertig EJ, Niu N, Zheng L, et al. A phase II study of allogeneic GM-CSF-transfected pancreatic tumor vaccine (GVAX) with ipilimumab as maintenance treatment for metastatic pancreatic cancer. *Clin Cancer Res* 2020;**26**:5129−39.
29. Chiang CL, Benencia F, Coukos G. Whole tumor antigen vaccines. *Semin Immunol* 2010;**22**:132−43.
30. Li Y, Zhang M, Wang X, Liu W, Wang H, Yang YG. Vaccination with CD47 deficient tumor cells elicits an antitumor immune response in mice. *Nat Commun* 2020;**11**:581.
31. Massague J, Sheppard D. TGF-beta signaling in health and disease. *Cell* 2023;**186**:4007−37.
32. Tauriello DVF, Sancho E, Batlle E. Overcoming TGFbeta-mediated immune evasion in cancer. *Nat Rev Cancer* 2022;**22**:25−44.
33. Sharma P, Zhang X, Ly K, Kim JH, Wan Q, Kim J, et al. Hyperglycosylation of prosaposin in tumor dendritic cells drives immune escape. *Science* 2024;**383**:190−200.
34. Chen J, Feng W, Sun M, Huang W, Wang G, Chen X, et al. TGF-β1-induced SOX18 elevation promotes hepatocellular carcinoma progression and metastasis through transcriptionally upregulating PD-L1 and CXCL12. *Gastroenterology* 2024;**167**:264−80.
35. Zhang D, Ni QQ, Liang QY, He LL, Qiu BW, Zhang LJ, et al. ASCL2 induces an immune excluded microenvironment by activating cancer-associated fibroblasts in microsatellite stable colorectal cancer. *Oncogene* 2023;**42**:2841−53.
36. Liu Y, Ji Y, Jiang R, Fang C, Shi G, Cheng L, et al. Reduced smooth muscle-fibroblasts transformation potentially decreases intestinal wound healing and colitis-associated cancer in ageing mice. *Signal Transduct Targeted Ther* 2023;**8**:294.
37. Kennel KB, Greten FR. The immune microenvironment of colorectal cancer. *Nat Rev Cancer* 2025;**25**:945−64.
38. Williams CJM, Peddle AM, Kasi PM, Seligmann JF, Roxburgh CS, Middleton GW, et al. Neoadjuvant immunotherapy for dMMR and pMMR colorectal cancers: therapeutic strategies and putative biomarkers of response. *Nat Rev Clin Oncol* 2024;**21**:839−51.
39. Gao Y, Zhang Y, Ma Y, Li X, Wang Y, Chen H, et al. NIR-II-activated whole-cell vaccine with ultra-efficient semiconducting diradical oligomers for breast carcinoma growth and metastasis inhibition. *Acta Pharm Sin B* 2025;**15**:1159−70.
40. Yang L, Yang J, Kleppe A, Danielsen HE, Kerr DJ. Personalizing adjuvant therapy for patients with colorectal cancer. *Nat Rev Clin Oncol* 2024;**21**:67−79.
41. Wang X, Xu H, Wang H, Hua R, Wu S, Xu J, et al. Construction strategies of whole tumor cell vaccines. *Biomater Sci* 2025;**13**:4885−97.
42. Dranoff G, Jaffee E, Lazenby A, Golumbek P, Levitsky H, Brose K, et al. Vaccination with irradiated tumor cells engineered to secrete murine granulocyte-macrophage colony-stimulating factor stimulates potent, specific, and long-lasting anti-tumor immunity. *Proc Natl Acad Sci U S A* 1993;**90**:3539−43.

43. Yu J, Shao B, Luo M, Du W, Nie W, Yang J, et al. Irradiated lactic acid-stimulated tumour cells promote the antitumour immunity as a therapeutic vaccine. *Cancer Lett* 2020;**469**:367−79.
44. Gottumukkala SB, Ganesan TS, Palanisamy A. Comprehensive molecular interaction map of TGFβ induced epithelial to mesenchymal transition in breast cancer. *npj Syst Biol Appl* 2024; **10**:53.
45. Nemunaitis J. GVAX (GMCSF gene modified tumor vaccine) in advanced stage non small cell lung cancer. *J Control Release* 2003;**91**: 225−31.
46. Lee SR, Park YK, Shin BA, Park HR. Effects of tumor vaccine expressing granulocyte-macrophage colony stimulating factor and interleukin-18 fusion on cancer cells and its possible application for cancer immunotherapy. *Cytokine* 2017;**89**:143−54.
47. Chiang CL, Coukos G, Kandalaft LE. Whole tumor antigen vaccines: where are we?. *Vaccines* 2015;**3**:344−72.
48. Xia L, Schrump DS, Gildersleeve JC. Whole-cell cancer vaccines induce large antibody responses to carbohydrates and glycoproteins. *Cell Chem Biol* 2016;**23**:1515−25.
49. Andersen BM, Ohlfest JR. Increasing the efficacy of tumor cell vaccines by enhancing cross priming. *Cancer Lett* 2012;**325**:155−64.
50. Lopez J, Powles T, Braiteh F, Siu LL, LoRusso P, Friedman CF, et al. Autogene cevumeran with or without atezolizumab in advanced solid tumors: a phase 1 trial. *Nat Med* 2025;**31**:152−64.